

Global Climate Changes as Forecast by Goddard Institute for Space Studies Three-Dimensional Model

J. HANSEN, I. FUNG, A. LACIS, D. RIND, S. LEBEDEFF, R. RUEDY, AND G. RUSSELL

NASA Goddard Space Flight Center, Goddard Institute for Space Studies, New York

P. STONE

Massachusetts Institute of Technology, Cambridge

We use a three-dimensional climate model, the Goddard Institute for Space Studies (GISS) model II with 8° by 10° horizontal resolution, to simulate the global climate effects of time-dependent variations of atmospheric trace gases and aerosols. Horizontal heat transport by the ocean is fixed at values estimated for today's climate, and the uptake of heat perturbations by the ocean beneath the mixed layer is approximated as vertical diffusion. We make a 100-year control run and perform experiments for three scenarios of atmospheric composition. These experiments begin in 1958 and include measured or estimated changes in atmospheric CO_2 , CH_4 , N_2O , chlorofluorocarbons (CFCs) and stratospheric aerosols for the period from 1958 to the present. Scenario A assumes continued exponential trace gas growth, scenario B assumes a reduced linear growth of trace gases, and scenario C assumes a rapid curtailment of trace gas emissions such that the net climate forcing ceases to increase after the year 2000. Principal results from the experiments are as follows: (1) Global warming to the level attained at the peak of the current interglacial and the previous interglacial occurs in all three scenarios; however, there are dramatic differences in the levels of future warming, depending on trace gas growth. (2) The greenhouse warming should be clearly identifiable in the 1990s; the global warming within the next several years is predicted to reach and maintain a level at least three standard deviations above the climatology of the 1950s. (3) Regions where an unambiguous warming appears earliest are low-latitude oceans, China and interior areas in Asia, and ocean areas near Antarctica and the north pole; aspects of the spatial and temporal distribution of predicted warming are clearly model-dependent, implying the possibility of model discrimination by the 1990s and thus improved predictions, if appropriate observations are acquired. (4) The temperature changes are sufficiently large to have major impacts on people and other parts of the biosphere, as shown by computed changes in the frequency of extreme events and by comparison with previous climate trends. (5) The model results suggest some near-term regional climate variations, despite the fixed ocean heat transport which suppresses many possible regional climate fluctuations; for example, during the late 1980s and in the 1990s there is a tendency for greater than average warming in the southeastern and central United States and relatively cooler conditions or less than average warming in the western United States and much of Europe. Principal uncertainties in the predictions involve the equilibrium sensitivity of the model to climate forcing, the assumptions regarding heat uptake and transport by the ocean, and the omission of other less-certain climate forcings.

1. INTRODUCTION

Studies of the climate impact of increasing atmospheric CO_2 have been made by means of experiments with three-dimensional (3D) climate models in which the amount of CO_2 was instantaneously doubled or quadrupled, with the model then integrated forward in time to a new steady state [Manabe and Wetherald, 1975; Manabe and Stouffer, 1980; Hansen et al., 1984; Washington and Meehl, 1984; Wilson and Mitchell, 1987]. These models all yield a large climate impact at equilibrium for doubled CO_2 , with global mean warming of surface air between about 2° and 5°C .

However, observations show that CO_2 is increasing gradually: its abundance was 315 parts per million by volume (ppmv) in 1958 when Keeling initiated accurate measurements and is now about 345 ppmv, with current mean annual increments of about 1.5 ppmv [Keeling et al., 1982]. Also there are at least two other known global radiative forcings of comparable magnitude: growth of several other trace gases [Wang et al., 1976; Lacis et al., 1981; Ramanathan et al., 1985] and variations in stratospheric aerosols due to

volcanic eruptions [Lamb, 1970; Mitchell, 1970; Schneider and Mass, 1975; Pollack et al., 1976; Hansen et al., 1978, 1980; Robock, 1981]. Still other radiative forcings, such as changes of solar irradiance, tropospheric aerosols, and land surface properties, may also be significant, but quantitative information is insufficient to define the trends of these forcings over the past several decades.

In this paper we study the response of a 3D global climate model to realistic rates of change of radiative forcing mechanisms. The transient response of the climate system on decadal time scales depends crucially on the response of the ocean, for which adequate understanding and dynamical models are not available. Our procedure is to use simple assumptions about ocean heat transport. Specifically we assume that during the next few decades the rate and pattern of horizontal ocean heat transport will remain unchanged and the rate of heat uptake by the ocean beneath the mixed layer can be approximated by diffusive mixing of heat perturbations. This "surprise-free" representation of the ocean provides a first estimate of the global transient climate response which can be compared both to observations and to future simulations developed with a dynamically interactive ocean. We include in this paper a description of the experiments and an analysis of computed temperature changes; other computed quantities, such as

Copyright 1988 by the American Geophysical Union.

Paper number 8DO369.
0148-0227/88/008D-0369\$05.00

changes in the atmospheric general circulation, precipitation, and sea ice cover will be presented elsewhere.

The climate model employed in our studies is described in section 2. Results of a 100-year control run of this model, with the atmospheric composition fixed, are briefly described in section 3. Three scenarios for atmospheric trace gases and stratospheric aerosols are defined in section 4. Results of the climate model simulations for these three scenarios are presented in section 5: section 5.1 examines the predicted global warming and the issue of when the global warming should exceed natural climate variability; section 5.2 examines the spatial distribution of predicted decadal temperature changes, and section 5.3 examines short-term and local temperature changes. In section 6, we summarize the model predictions and discuss the principal caveats and assumptions upon which the results depend.

Our transient climate experiments were initiated in early 1983, being run as a background job on the GISS mainframe computer, a general-purpose machine (Amdahl V-6) of mid-1970s vintage. Results for scenario A were reported at a conference in June 1984 [Shands and Hoffman, 1987], and results from all scenarios were presented at several later conferences.

2. CLIMATE MODEL

The atmospheric component of the global climate model we employ is described and its abilities and limitations for simulating today's climate are documented as model II (Hansen et al. [1983], hereafter referred to as paper 1). The model solves the simultaneous equations for conservation of energy, momentum, mass, and water vapor and the equation of state on a coarse grid with nine atmospheric layers and horizontal resolution 8° latitude by 10° longitude. The radiation calculation includes the radiatively significant atmospheric gases, aerosols, and cloud particles. Cloud cover and height are computed, but cloud opacity is specified as a function of cloud type, altitude, and thickness. The diurnal and seasonal cycles are included. The ground hydrology and surface albedo depend upon the local vegetation. Snow depth is computed, and snow albedo includes effects of snow age and masking by vegetation. The equilibrium sensitivity of this model for doubled CO_2 (315 ppmv \rightarrow 630 ppmv) is 4.2°C for global mean surface air temperature (Hansen et al. [1984], hereafter referred to as paper 2). This is within, but near the upper end of, the range $3^\circ \pm 1.5^\circ\text{C}$ estimated for climate sensitivity by National Academy of Sciences committees [Charney, 1979; Smagorinsky, 1982], where their range is a subjective estimate of the uncertainty based on climate-modeling studies and empirical evidence for climate sensitivity. The sensitivity of our model is near the middle of the range obtained in recent studies with general circulation models (GCMs) [Washington and Meehl, 1984; paper 2, 1984; Manabe and Wetherald, 1987; Wilson and Mitchell, 1987].

Ocean temperature and ice cover were specified climatologically in the version of model II documented in paper 1. In the experiments described here and in paper 2, ocean temperature and ice cover are computed based on energy exchange with the atmosphere, ocean heat transport, and the ocean's heat capacity. The treatments of ocean temperature and ice cover are nearly the same here as in paper 2, with the following exception. In paper 2, since the

objective was to study equilibrium ($t \rightarrow \infty$) climate changes, computer time was saved by specifying the maximum mixed layer depth as 65 m and by allowing no exchange of heat between the mixed layer and the deeper ocean. In this paper, since we are concerned with the transient climate response, we include the entire mixed layer with seasonally varying depth specified from observations, as described in Appendix A, and (except in the control run) we allow diffusive vertical heat transport beneath the level defined by the annual maximum mixed layer depth. The global mean depth of this level is about 125 m and the effective global diffusion coefficient beneath it is about $1 \text{ cm}^2 \text{ s}^{-1}$.

The horizontal transport of heat in the ocean is specified from estimates for today's ocean, varying seasonally at each grid point, as described in Appendix A. In our experiments with changing atmospheric composition, we keep the ocean horizontal heat transport (and the mixed layer depth) identical to that in the control run, i.e., no feedback of climate change on ocean heat transport is permitted in these experiments. Our rationale for this approach as a first step is that it permits a realistic atmospheric simulation and simplifies analysis of the experiments. Initial experiments with an idealized interactive atmosphere/ocean model suggest that the assumption of no feedback may be a good first approximation for small climate perturbations in the direction of a warmer climate [Bryan et al., 1984; Manabe and Bryan, 1985]. In addition, experiments with a zonal average heat balance model suggest that the global average climate sensitivity does not depend strongly on the feedback in the ocean heat transport [Wang et al., 1984]. However, we stress that this "surprise-free" representation of the ocean excludes the effects of natural variability of ocean transports and the possibility of switches in the basic mode of ocean circulation. Broecker et al. [1985], for example, have suggested that sudden changes in the rate of deepwater formation may be associated with oscillations of the climate system. Discussions of the transient ocean response have been given by Schneider and Thompson [1981], Bryan et al. [1984], and others. We consider our simple treatment of the ocean to be only a first step in studying the climate response to a slowly changing climate forcing, one which must be compared with results from dynamically interactive ocean models when such models are applied to this problem.

3. A 100 YEAR CONTROL RUN

A 100-year control run of the model was carried out with the atmospheric composition fixed at estimated 1958 values. Specifically, atmospheric gases which are time-dependent in later experiments are set at the values 315 ppmv for CO_2 , 1400 parts per billion by volume (ppbv) for CH_4 , 292.6 ppbv for N_2O , 15.8 parts per trillion by volume (pptv) for CCl_3F (F-11), and 50.3 pptv for CCl_2F_2 (F-12).

The ocean mixed layer depth varies geographically and seasonally, based on climatological data specified in Appendix A. No heat exchange across the level defined by the annual maximum mixed layer depth was permitted in the control run described in this section. The purpose of this constraint was to keep the response time of the model short enough that it was practical to extend the model integration over several time constants, thus assuring near-equilibrium conditions. The isolated mixed layer response time is 10–20

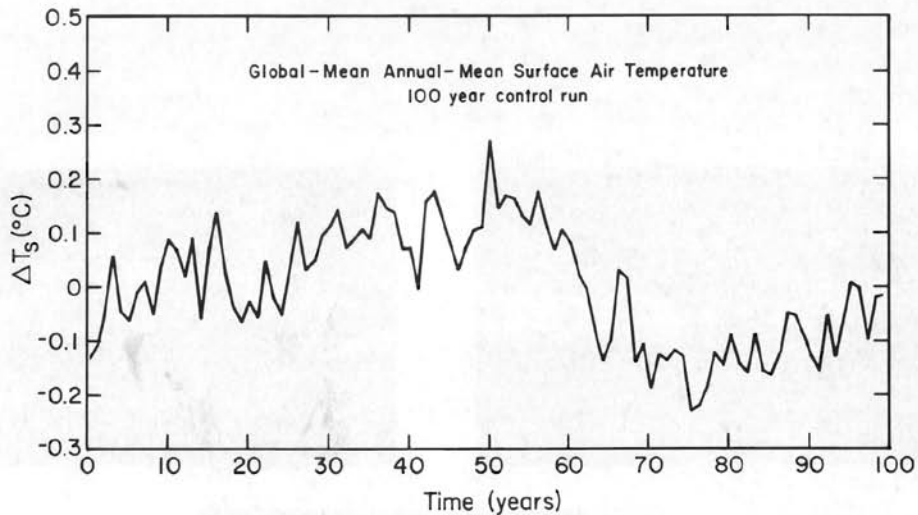


Fig. 1. Global-mean annual-mean surface air temperature trend in the 100-year control run.

years for a climate sensitivity of 4°C for doubled CO_2 , as shown in paper 2. Note that the seasonal thermocline (i.e., the water between the base of the seasonal mixed layer and the annual maximum mixed layer depth) can have a different temperature each year; this heat storage and release can affect the interannual variability of surface temperature.

The variation of the global-mean annual-mean surface air temperature during the 100-year control run is shown in Figure 1. The global mean temperature at the end of the run is very similar to that at the beginning, but there is substantial unforced variability on all time scales that can be examined, that is, up to decadal time scales. Note that an unforced change in global temperature of about 0.4°C (0.3°C , if the curve is smoothed with a 5-year running mean) occurred in one 20-year period (years 50–70). The standard deviation about the 100-year mean is 0.11°C . This unforced variability of global temperature in the model is only slightly smaller than the observed variability of global surface air temperature in the past century, as discussed in section 5. The conclusion that unforced (and unpredictable) climate variability may account for a large portion of climate change has been stressed by many researchers; for example, Lorenz [1968], Hasselmann [1976] and Robock [1978].

The spatial distribution of the interannual variability of temperature in the model is compared with observational data in Plate 1. The geographical distribution of surface air temperature variability is shown in Plate 1a for the model and Plate 1b for observations. The standard deviation ranges from about 0.25°C at low latitudes to more than 1°C at high latitudes in both the model and observations. The model's variability tends to be larger than observed over continents; this arises mainly from unrealistically large model variability (by about a factor of 2) over the continents in summer, as shown by the seasonal graphs of Hansen and Lebedeff [1987]. The interannual variability of the zonal mean surface air temperature, as a function of latitude and month, is shown in Plate 1c and 1d for the model and observations. The seasonal distribution of variability in the model is generally realistic, except that

the summer minimum in the northern hemisphere occurs about 1 month early. The interannual variability of temperature as a function of height is more difficult to check, because observations of sufficient accuracy are limited to radiosonde data. J. Angell (private communication, 1987) has analyzed data from 63 radiosonde stations, averaged the temperature change zonally, and tabulated the data with a resolution of seven latitude bands and four heights, the lowest of these heights being the surface air; the interannual variability of the results is shown in Plate 1f. Reasons for smaller variability in the model, Plate 1e, probably include (1) identical ocean heat transport every year, which inhibits occurrence of phenomena such as El Niño and the associated variability of upper air temperature, and (2) stratospheric drag in the upper model layer of the nine-layer model II, which reduces variability in the stratosphere and upper troposphere, as shown by experiments with a 23-layer version of the model which has its top at 85 km [Rind et al., 1988].

We use these interannual variabilities in section 5 to help estimate the significance of predicted climate trends and to study where it should be most profitable to search for early evidence of greenhouse climate effects. We defer further discussion of model variability and observed variability to that section.

4. RADIATIVE FORCING IN SCENARIOS A, B AND C

4.1. Trace Gases

We define three trace gas scenarios to provide an indication of how the predicted climate trend depends upon trace gas growth rates. Scenario A assumes that growth rates of trace gas emissions typical of the 1970s and 1980s will continue indefinitely; the assumed annual growth averages about 1.5% of current emissions, so the net greenhouse forcing increases exponentially. Scenario B has decreasing trace gas growth rates, such that the annual increase of the greenhouse climate forcing remains approximately constant at the present level. Scenario C drastically reduces trace gas growth between 1990 and 2000 such that the greenhouse climate forcing ceases to increase after 2000.

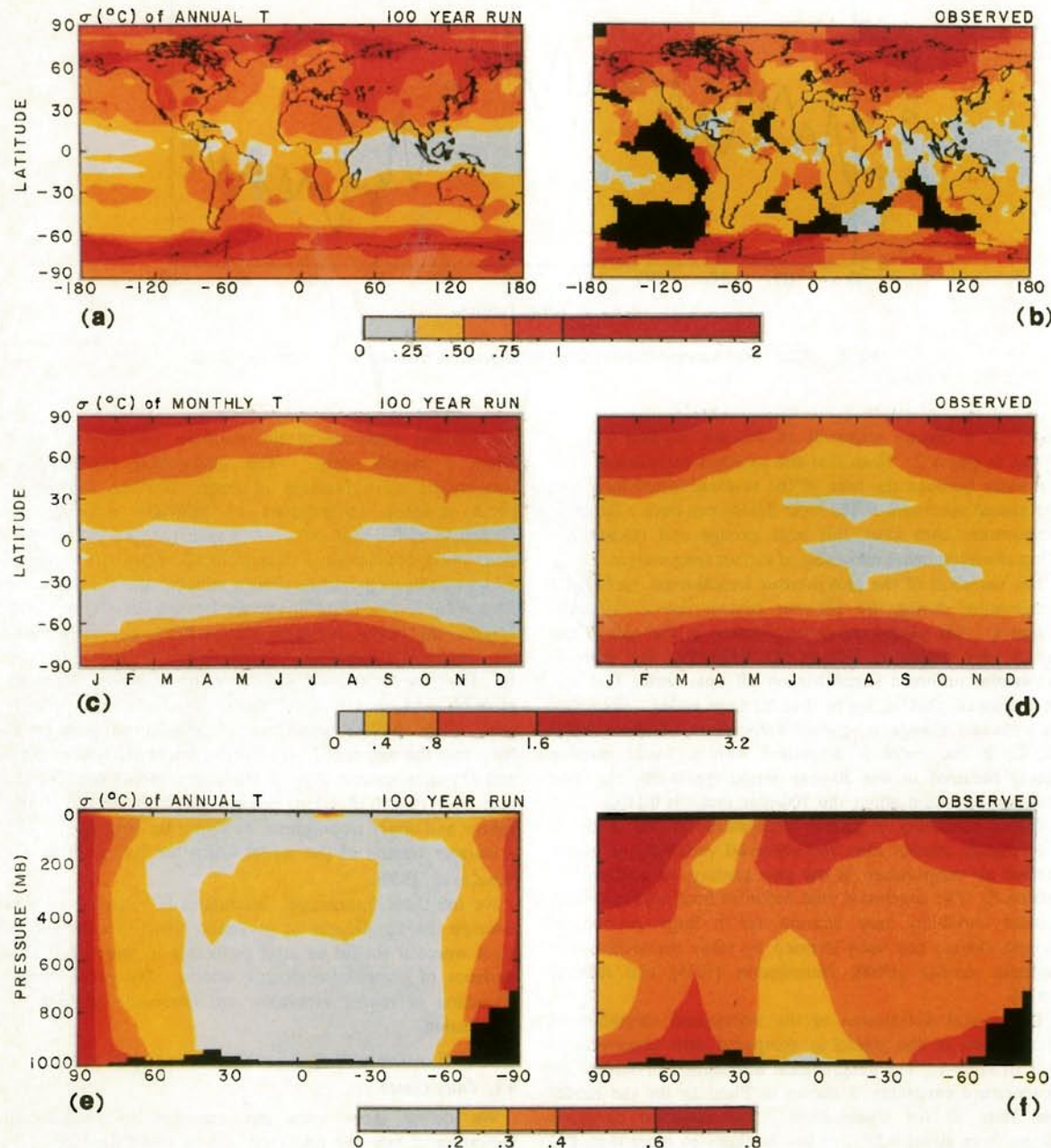


Plate 1. (Left) Interannual variability (standard deviation) of temperature in the 100-year control run and (right) as estimated from observations. Plates 1a, 1b, 1c, and 1d show the interannual variability of surface air temperature, and Plates 1e and 1f show the interannual variability of the longitude-integrated upper air temperature. (b) and (d) are based on 1951–1980 observations at meteorological stations analyzed by Hansen and Lebedeff [1987]. Plate 1f is based on 1958–1985 radiosonde data analyzed by Angell [1986]. Regions without data are black.

The range of climate forcings covered by the three scenarios is further increased by the fact that scenario A includes the effect of several hypothetical or crudely estimated trace gas trends (ozone, stratospheric water vapor, and minor chlorine and fluorine compounds) which are not included in scenarios B and C.

These scenarios are designed to yield sensitivity experiments for a broad range of future greenhouse forcings. Scenario A, since it is exponential, must eventually be on the high side of reality in view of finite resource constraints and environmental concerns, even though the growth of emissions in scenario A ($\approx 1.5\% \text{ yr}^{-1}$) is less than the rate typical of the past century ($\approx 4\% \text{ yr}^{-1}$). Scenario C is a more drastic curtailment of emissions than has generally been imagined; it represents elimination of chlorofluorocarbon (CFC) emissions by 2000 and reduction of CO_2 and other trace gas emissions to a level such that the annual growth rates are zero (i.e., the sources just balance the sinks) by the year 2000. Scenario B is perhaps the most plausible of the three cases.

The abundances of the trace gases in these three scenarios are specified in detail in Appendix B. The net greenhouse forcing, ΔT_o , for these scenarios is illustrated in Figure 2; ΔT_o is the computed temperature change at equilibrium ($t \rightarrow \infty$) for the given change in trace gas abundances, with no climate feedbacks included [paper 2]. Scenario A reaches a climate forcing equivalent to doubled CO_2 in about 2030, scenario B reaches that level in about 2060, and scenario C never approaches that level. Note that our scenario A goes approximately through the middle of the range of likely climate forcing estimated for the year 2030 by Ramanathan et al. [1985], and scenario B is near the lower limit of their estimated range. Note also that the forcing in scenario A exceeds that for scenarios B and C for the period from 1958 to the present, even though the forcing in that period is nominally based on observations; this is because scenario A includes a forcing for some speculative trace gas changes in addition to the measured ones (see Appendix B).

Our climate model computes explicitly the radiative forcing due to each of the above trace gases, using the correlated k -distribution method [paper 1]. However, we anticipate that the climate response to a given global radiative forcing ΔT_o is similar to first order for different gases, as supported by calculations for different climate forcings in paper 2. Therefore results obtained for our three scenarios provide an indication of the expected climate response for a very broad range of assumptions about trace gas trends. The forcing for any other scenario of atmospheric trace gases can be compared to these three cases by computing $\Delta T_o(t)$ with formulas provided in Appendix B.

4.2. Stratospheric Aerosols

Stratospheric aerosols provide a second variable climate forcing in our experiments. This forcing is identical in all three experiments for the period 1958–1985, during which time there were two substantial volcanic eruptions, Agung in 1963 and El Chichón in 1982. In scenarios B and C, additional large volcanoes are inserted in the year 1995 (identical in properties to El Chichón), in the year 2015 (identical to Agung), and in the year 2025 (identical to El Chichón), while in scenario A no additional volcanic aerosols

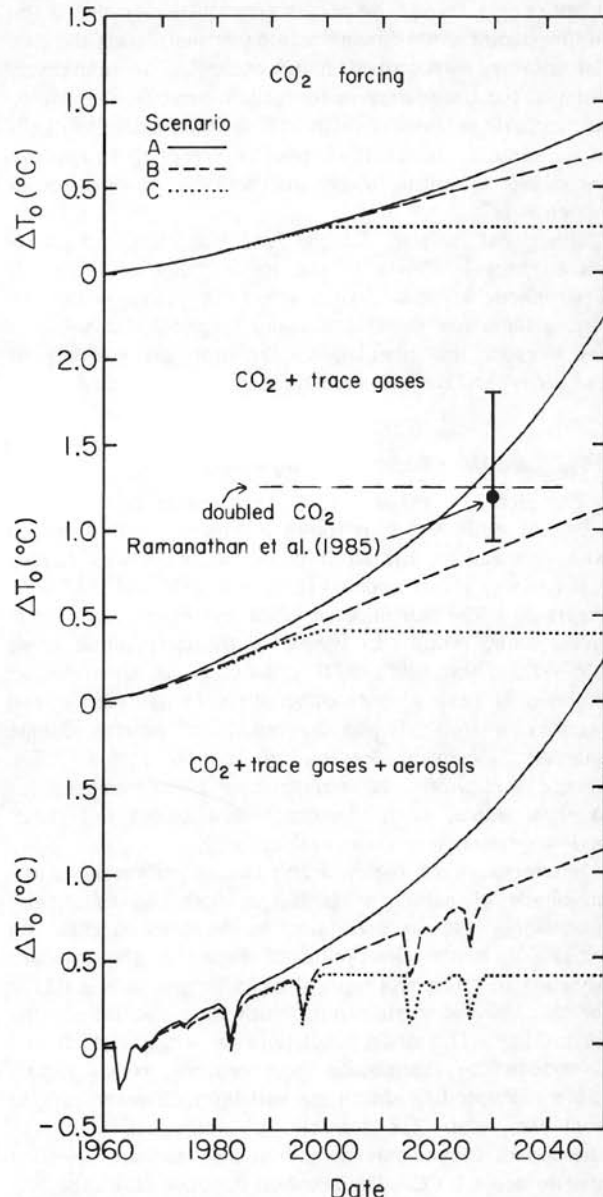


Fig. 2. Greenhouse forcing for trace gas scenarios A, B, and C, as described in the text. ΔT_o is the equilibrium greenhouse warming for no climate feedbacks. The doubled CO_2 level of forcing, $\Delta T_o \approx 1.25^\circ\text{C}$, occurs when the CO_2 and trace gases added after 1958 provide a forcing equivalent to doubling CO_2 from 315 ppm to 630 ppm. The CO_2 plus trace gas forcing estimated by Ramanathan et al. [1985] for the year 2030 is also illustrated.

are included after those from El Chichón have decayed to the background stratospheric aerosol level. The stratospheric aerosols in scenario A are thus an extreme case, amounting to an assumption that the next few decades will be similar to the few decades before 1963, which were free of any volcanic eruptions creating large stratospheric optical depths. Scenarios B and C in effect use the assumption that the mean stratospheric aerosol optical depth during the next few decades will be comparable to that in the volcanically active period 1958–1985.

The radiative forcing due to stratospheric aerosols depends upon their physical properties and global distribution. Sufficient observational data on stratospheric

opacities and aerosol properties are available to define the stratospheric aerosol forcing reasonably well during the past few decades, as described in Appendix B. We subjectively estimate the uncertainty in the global mean forcing due to stratospheric aerosols as about 25% for the period from 1958 to the present. It should be possible eventually to improve the estimated aerosol forcing for the 1980s, as discussed in Appendix B.

The global radiative forcing due to aerosols and greenhouse gases is shown in the lower panel of Figure 2. Stratospheric aerosols have a substantial effect on the net forcing for a few years after major eruptions, but within a few decades the cumulative CO_2 /trace gas warming in scenarios A and B is much greater than the aerosol cooling.

5. TRANSIENT SIMULATIONS

5.1. Global Mean Surface Air Temperature

The global mean surface air temperature computed for scenarios A, B, and C is shown in Figure 3 and compared with observations, the latter based on analyses of Hansen and Lebedeff [1987] updated to include 1986 and 1987 data. Figure 3a is the annual mean result and Figure 3b is the 5-year running mean. In Figure 3a the temperature range 0.5°–1.0°C above 1951–1980 climatology is noted as an estimate of peak global temperatures in the current and previous interglacial periods, based on several climate indicators [National Academy of Sciences (NAS), 1975]; despite uncertainties in reconstructing global temperatures at those times, it is significant that recent interglacial periods were not much warmer than today.

Interpretation of Figure 3 requires quantification of the magnitude of natural variability in both the model and observations and the uncertainty in the measurements. As mentioned in the description of Figure 1, the standard deviation of the model's global mean temperature is 0.11°C for the 100-year control run, which does not include the thermocline. The model simulations for scenarios A, B, and C include the thermocline heat capacity, which slightly reduces the model's short-term variability; however, judging from the results for scenario A, which has a smooth variation of climate forcing, the model's standard deviation remains about 0.1°C. The standard deviation about the 100-year mean for the observed surface air temperature change of the past century (which has a strong trend) is 0.20°C; it is 0.12°C after detrending [Hansen et al., 1981]. The 0.12°C detrended variability of observed temperatures was obtained as the average standard deviation about the ten 10-year means in the past century; if, instead, we compute the average standard deviation about the four 25-year means, this detrended variability is 0.13°C. For the period 1951–1980, which is commonly used as a reference period, the standard deviation of annual temperature about the 30-year mean is 0.13°C. It is not surprising that the variability of the observed global temperature exceeds the variability in the GCM control run, since the latter contains no variable climate forcings such as changes of atmospheric composition or solar irradiance; also specification of ocean heat transport reduces interannual variability due to such phenomena as El Niño/Southern Oscillation events. Finally, we note that the 1σ error in the observations due to incomplete coverage of stations is about 0.05°C for the period from 1958 to the present [Hansen and Lebedeff,

1987], which does not contribute appreciably to the variability (standard deviation) of the observed global temperature. We conclude that, on a time scale of a few decades or less, a warming of about 0.4°C is required to be significant at the 3σ level (99% confidence level).

There is no obviously significant warming trend in either the model or observations for the period 1958–1985. During the single year 1981, the observed temperature nearly reached the 0.4°C level of warming, but in 1984 and 1985 the observed temperature was no greater than in 1985. Early reports show that the observed temperature in 1987 again approached the 0.4°C level [Hansen and Lebedeff, 1988], principally as a result of high tropical temperatures associated with an El Niño event which was present for the full year. Analyses of the influence of previous El Niños on northern hemisphere upper air temperatures [Peixoto and Oort, 1984] suggest that global temperature may decrease in the next year or two.

The model predicts, however, that within the next several years the global temperature will reach and maintain a 3σ level of global warming, which is obviously significant. Although this conclusion depends upon certain assumptions, such as the climate sensitivity of the model and the absence of large volcanic eruptions in the next few years, as discussed in Section 6, it is robust for a very broad range of assumptions about CO_2 and trace gas trends, as illustrated in Figure 3.

Another conclusion is that global warming to the level attained at the peak of the current interglacial and the previous interglacial appears to be inevitable; even with the drastic, and probably unrealistic, reductions of greenhouse forcings in scenario C, a warming of 0.5°C is attained within the next 15 years. The eventual warming in this scenario would exceed 1°C, based on the forcing illustrated in Figure 2 and the feedback factor $f \approx 3.4$ for our GCM [paper 2]. The 1°C level of warming is exceeded during the next few decades in both scenarios A and B; in scenario A that level of warming is reached in less than 20 years and in scenario B it is reached within the next 25 years.

5.2. Spatial Distribution of Decadal Temperature Changes

5.2.1. Geographical distribution. The geographical distribution of the predicted surface air temperature change for the intermediate scenario B is illustrated in the left-hand column of Plate 2 for the 1980s, 1990s and 2010s. The right-hand column is the ratio of this decadal temperature change to the interannual variability (standard deviation) of the local temperature in the 100-year control run (Plate 1a). Since the interannual variability of surface air temperature in the model is reasonably similar to the variability in the real world (Plate 1b), this ratio provides a practical measure of when the predicted mean greenhouse warming is locally significant.

Averaged over the full decade of the 1980s, the model shows a tendency toward warming, but in most regions the decadal-mean warming is less than the interannual variability of the annual mean. In the 1990s the decadal-mean warming is comparable to the interannual variability for many regions, and by the 2010s almost the entire globe has very substantial warming, as much as several times the interannual variability of the annual mean.

The warming is generally greater over land than over the

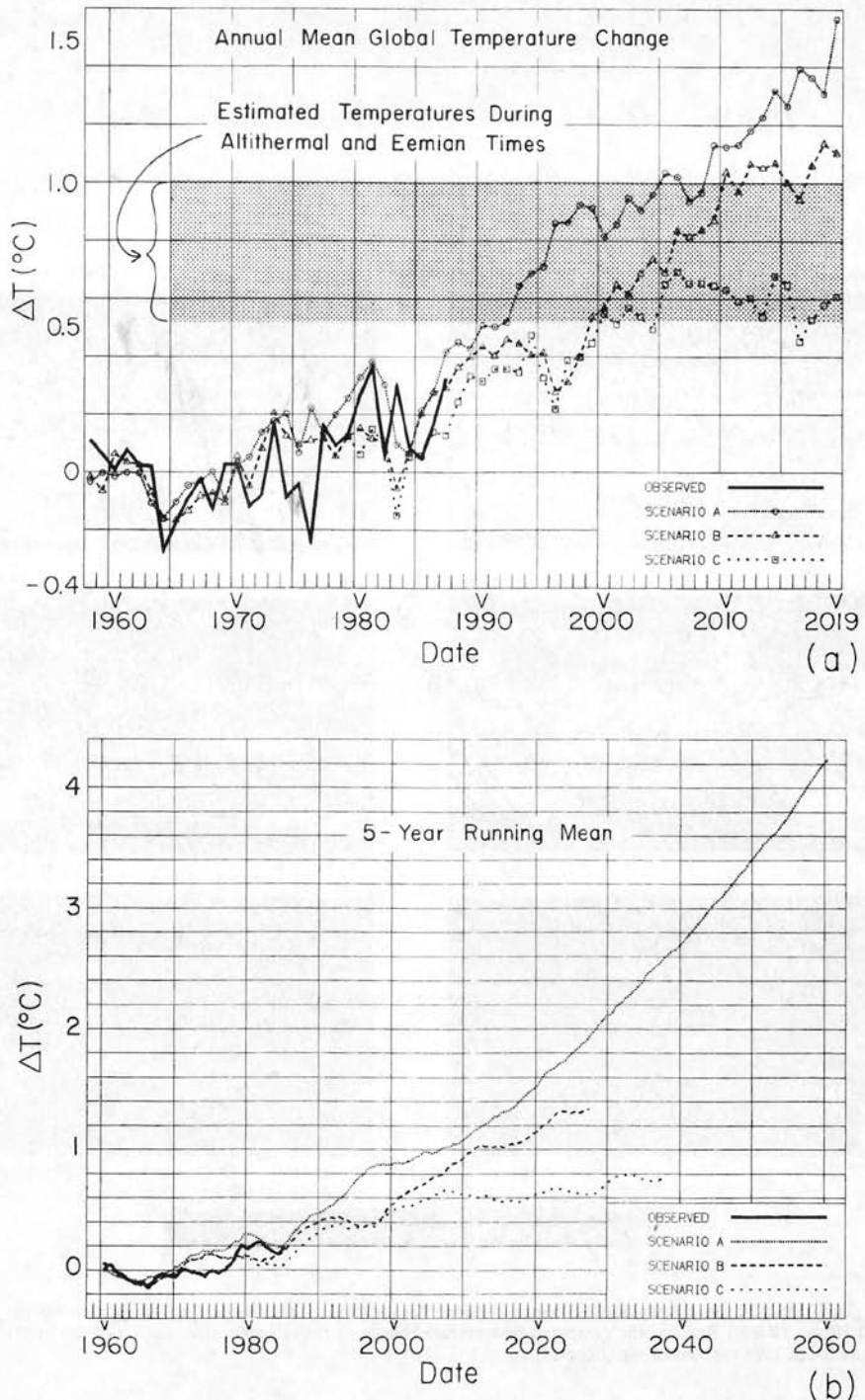


Fig. 3. Annual-mean global surface air temperature computed for scenarios A, B and C. Observational data is from Hansen and Lebedeff [1987, 1988]. The shaded range in Figure 3a is an estimate of global temperature during the peak of the current and previous interglacial periods, about 6,000 and 120,000 years before present, respectively. The zero point for observations is the 1951–1980 mean [Hansen and Lebedeff, 1987]; the zero point for the model is the control run mean. (a) Annual mean global temperature change, 1958–2019; (b) Five-year running mean, 1960–2060.

ocean and is greater at high latitudes than at low latitudes, being especially large in regions of sea ice. Regions where the warming shows up most prominently in our model, relative to the interannual variability, are (1) low-latitude

ocean regions where the surface response time is small (see Figure 15 of paper 2) because of a shallow ocean mixed layer and small thermocline diffusion, specifically regions such as the Caribbean, the East Indies, the Bay of Bengal,

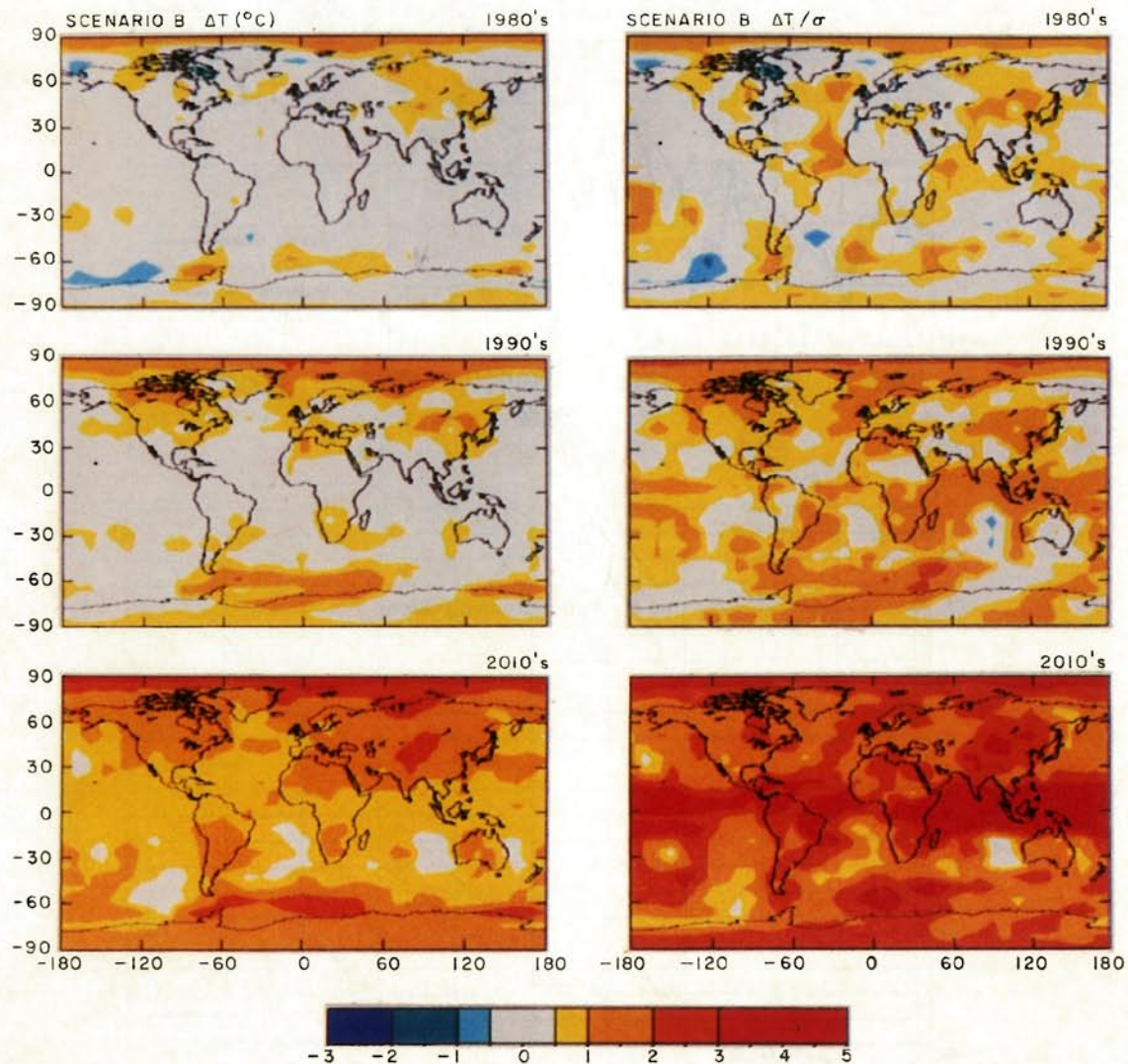


Plate 2. (Left) Decadal mean temperature change obtained for scenario B, relative to the control run, for the 1980s, 1990s and 2010s. (Right) Ratio of the computed temperature change to the interannual variability of the annual mean temperature in the 100-year control run (Plate 1a).

and large parts of the Indian, Atlantic and Pacific Oceans near or just north of the equator, (2) China, where the model's variability is twice as large as the observed variability; (compare with Plate 1) and the interior downwind portion of the Eurasian continent, especially the Kazakh-Tibet-Mongolia-Manchuria region, and (3) ocean areas near Antarctica and the north pole, where sea ice provides a positive climate feedback. The regions predicted to have earliest detectability of greenhouse warming are undoubtedly model dependent to some extent; as discussed later, this model dependence, in conjunction with global observations, may soon provide valuable information on climate mechanisms.

The predicted signal-to-noise ratio ($\Delta T/\sigma$) is generally smaller at any given geographical location than it is for the global mean (Figure 3), because the noise is significantly reduced in the global average. Thus for the single purpose of detecting a greenhouse warming trend, the global mean temperature provides the best signal. The geographical distribution of the predicted global temperature change also can be used for "optimal weighting" of global data to enhance early detection of a climate trend [Bell, 1982], but the impact of such weighting is modest and model dependent.

Our results suggest that the geographical patterns of model predicted temperature change, in combination with observations, should become valuable soon for discriminating among alternative model results, thus providing information on key climate processes which in turn may help narrow the range for predictions of future climate. For example, Plate 2 shows a strong warming trend in sea ice regions bordering the Antarctic continent; on the contrary, the ocean atmosphere model of S. Manabe and K. Bryan (private communication, 1987) shows cooling in this region for the first few decades after an instant doubling of atmospheric CO₂. The contrary results probably arise from different heat transports by the oceans in the GISS and Geophysical Fluid Dynamics Laboratory (GFDL) models. As a second example, our model yields a strong warming trend at low latitudes as does the British Meteorological Office (BMO) model [Wilson and Mitchell, 1987], while the GFDL and National Center for Atmospheric Research (NCAR) models [Washington and Meehl, 1984] yield minimal warming at low latitudes. The contrary results in this case may arise from the treatments of moist convection, as the GISS and BMO models use penetrative convection schemes and the GFDL and NCAR models use a moist adiabatic adjustment. Judging from Plate 2, the real world laboratory may provide empirical evidence relating to such climate mechanisms by the 1990s.

5.2.2. Latitude-season distribution. The dependence of the predicted temperature changes on season is investigated in Plate 3, which shows the predicted surface air temperature change for scenario B as a function of latitude and month (left-hand side) and the ratio of this to the model's interannual variability (right-hand side). Although the largest ΔT s are at high latitudes and in the winter, the variability is also largest at high latitudes and in the winter. Considering also the differences between the model's variability and observed variability (Plate 1), Plate 3 suggests that the best place to look for greenhouse warming in the surface air may be at middle and low latitudes in both hemispheres, with the signal-to-noise in summer being as great or greater than in winter.

5.2.3. Latitude-height distribution. The dependence of the predicted temperature changes on altitude is investigated in Plate 4, which shows the predicted upper air temperature change as a function of pressure and latitude (left-hand side) and the ratio of this to the model's interannual variability (right-hand side). Although the predicted greenhouse warming in our climate model is greater in the upper troposphere at low latitudes than it is at the surface, the signal-to-noise ratio does not have a strong height dependence in the troposphere. The dominant characteristic of the predicted atmospheric temperature change is stratospheric cooling with tropospheric warming. This characteristic could be a useful diagnostic for the greenhouse effect, since, for example, a tropospheric warming due to increased solar irradiance should be accompanied by only a slight stratospheric cooling (compare with Figure 4 in paper 2). However, the large signal-to-noise for the stratospheric cooling in Plate 4 is partly an artifact of the unrealistically small variability at stratospheric levels in our nine-layer model; the model predictions there need to be studied further with a model which has more appropriate vertical structure.

5.2.4. Comparisons with observations. Global maps of observed surface air temperature for the first 7 years of the 1980's show measurable warming, compared to observations for 1951–1980, especially in central Asia, northern North America, the tropics, and near some sea ice regions [Hansen et al., 1987]. There are general similarities between these observed patterns of warming and the model results (Plate 2); the magnitude of the warming is typically in the range 0.5–1.0 σ defined in Plate 1. Perhaps a more quantitative statement could be made by using the observational and model data in detection schemes which optimally weight different geographical regions [e.g., Bell, 1982; Barnett, 1986]. The significance of such comparisons should increase after data are available for the last few years of the 1980s, which are particularly warm in the model. However, information from the pattern of surface warming is limited by the fact that similar patterns can result from different climate forcings [Manabe and Wetherald, 1975; paper 2].

Comparisons of temperature changes as a function of height may be more diagnostic of the greenhouse effect, as mentioned earlier. Analysis of radiosonde data for the period 1960–1985 by Angell [1986] suggests a global warming of about 0.3°C in the 300 to 850-mbar region and a cooling of about 0.5°C in the 100 to 300-mbar and 50 to 100-mbar regions over that 25-year period. Although the warming in the lower troposphere and cooling in the stratosphere are consistent with our model results (Plate 4), the upper tropospheric (100–300 mbar) cooling is not. The temperature changes are about 0.5–1 σ , based on the natural variability in the model and observations (Plate 1). Note that our illustrated model results are for the period 1980–1989.

None of the climate models which have been applied to the greenhouse climate problem yield upper tropospheric cooling as found in observations by Angell [1986]. If this characteristic of the observations persists over the next several years, as the modeled temperature changes reach higher levels of mathematical significance, it will suggest either a common problem in the models or that we need to include additional climate forcing mechanisms in the analyses. Although the trend in the observations is not yet clear, it is perhaps worthwhile to point out examples of

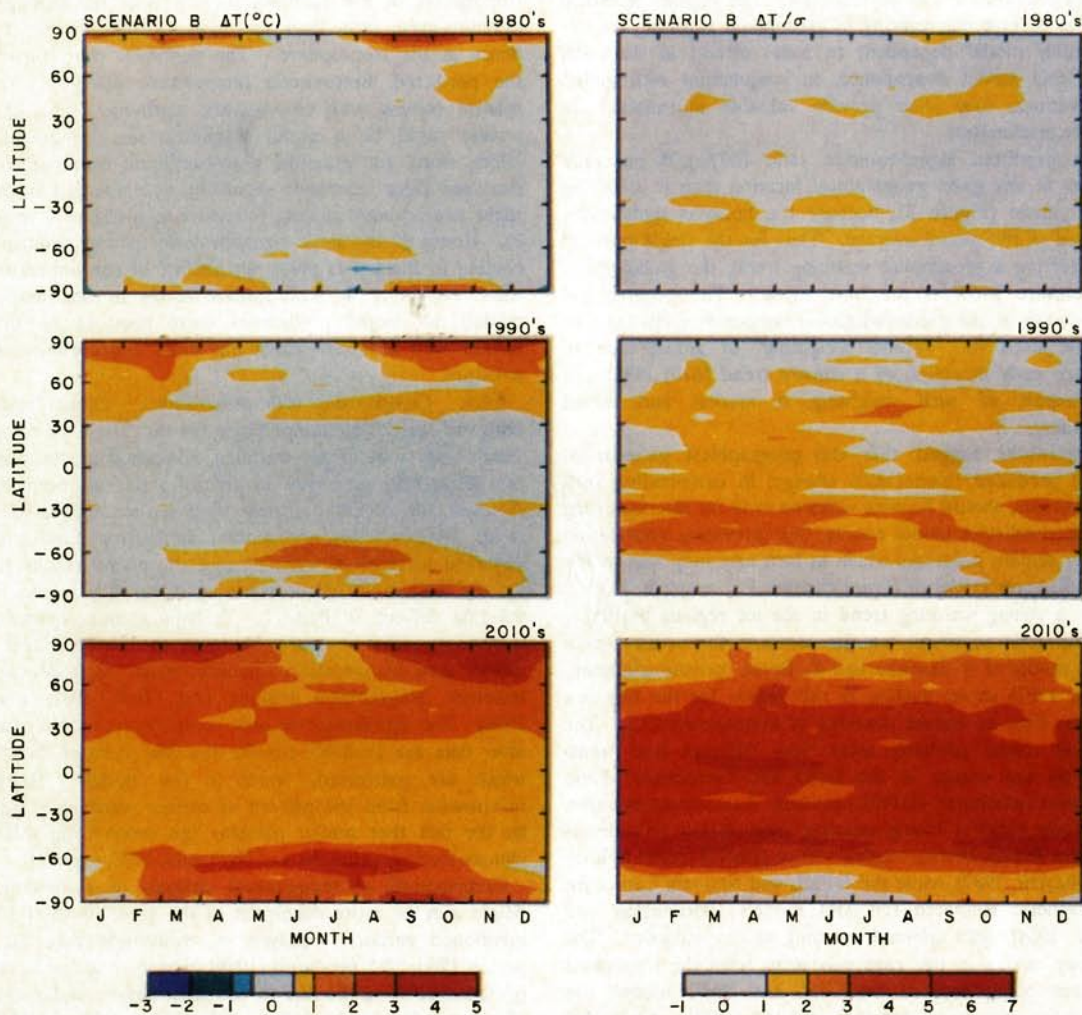


Plate 3. (Left) Decadal mean temperature change for scenario B as a function of latitude and season, for the 1980s, 1990s and 2010s. (Right) Ratio of the computed temperature change to the interannual variability of the monthly mean temperature in the 100-year control run (Plate 1c).

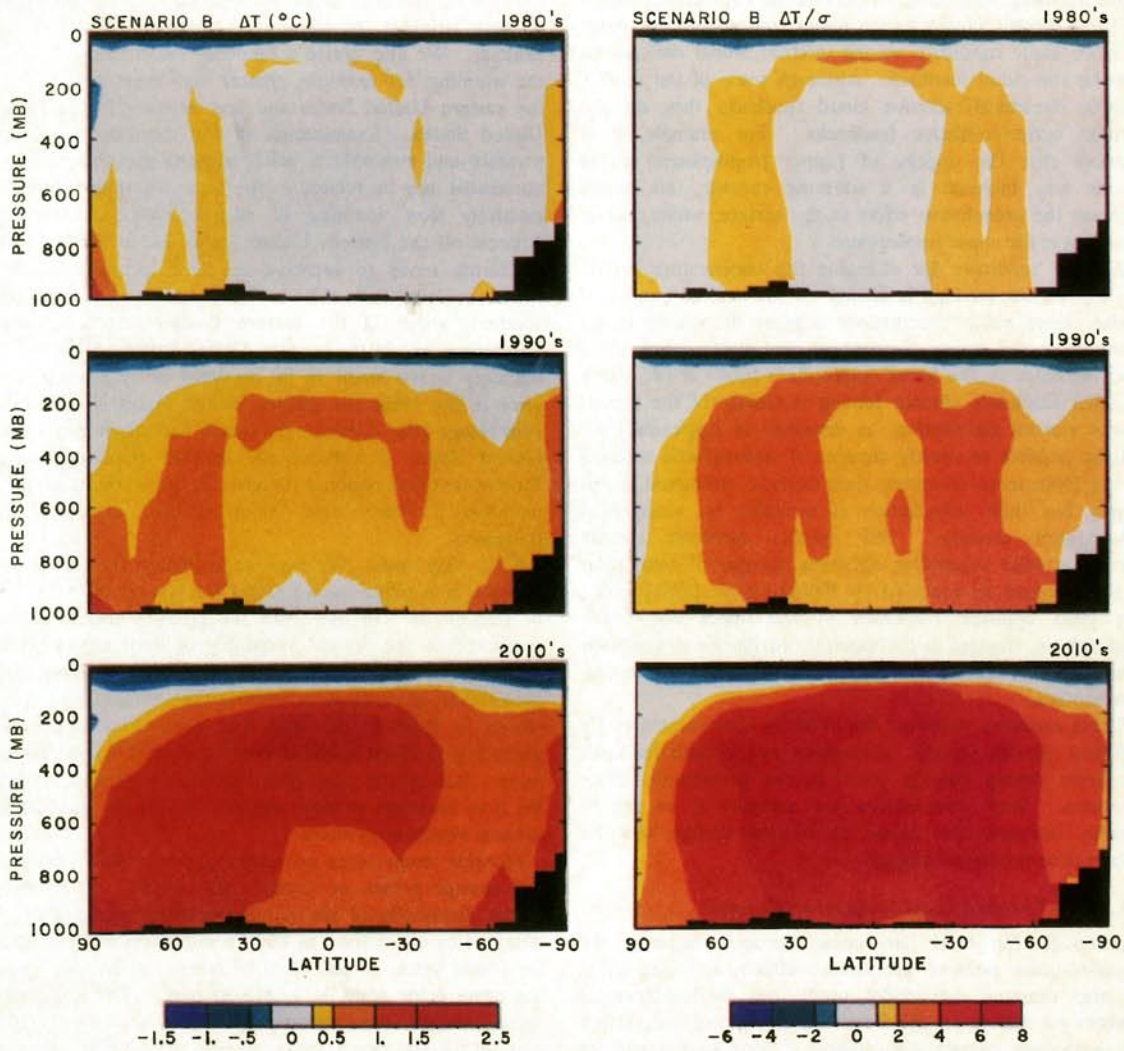


Plate 4. (Left) Decadal mean temperature change for scenario B as a function of pressure and latitude, for the 1980s, 1990s and 2010s. (Right) Ratio of the computed temperature change to the interannual variability of the annual mean temperature in the 100-year control run (Plate 1e).

mechanisms which could produce a discrepancy between model and observations.

Concerning possible common model problems, a prime a priori candidate would be the modeling of moist convection, since it is a principal process determining the vertical temperature gradient. However, the treatment of convection in the models (GFDL, GISS, NCAR and BMO) ranges from moist adiabatic adjustment to penetrating convection, and all of these models obtain strong upper tropospheric warming. A more likely candidate among internal model deficiencies may be the cloud feedback. Although some of the models include dynamical/radiative cloud feedback, they do not include optical/radiative feedbacks. For example, it is possible that the opacity of (upper tropospheric) cirrus clouds may increase in a warming climate; this would increase the greenhouse effect at the surface, while causing a cooling in the upper troposphere.

A good candidate for changing the temperature profile among climate forcings is change of the vertical profile of ozone, since some observations suggest decreasing ozone amounts in the upper troposphere and stratosphere along with increases in the lower troposphere [Bolle *et al.*, 1986]. Another candidate climate forcing is change of the atmospheric aerosol distribution; as discussed in Appendix B, it will be possible to specify changes of stratospheric aerosols in the 1980s more accurately than we have attempted in this paper, but little information is available on changes in tropospheric aerosols. Still another candidate climate forcing is solar variability; although changes of total solar irradiance such as reported by Willson *et al.* [1986] would not yield opposite responses in the upper and lower troposphere, changes in the spectral distribution of the solar irradiance may have a more complicated effect on temperature profiles.

These examples point out the need for observations of the different climate forcing mechanisms and climate feedback processes during coming years as the greenhouse effect increases. Such observations are essential if we are to reliably interpret the causes of climate change and the implications for further change.

5.3. Short-Term and Local Temperature Changes

Although long-term large-area averages increase the signal-to-noise ratio of greenhouse effects, it is important to also examine the model predictions for evidence of greenhouse effects on the frequency and global distribution of short-term climate disturbances. Such studies will be needed to help answer practical questions, such as whether the greenhouse effect has a role in observed local and regional climate fluctuations.

We illustrate here samples of model results at seasonal and monthly temporal resolutions, and we estimate the effect of the temperature changes on the frequency of extreme temperatures at specific locales. The object is not to make predictions for specific years and locations, but rather to provide some indication of the magnitude of practical impacts of the predicted temperature changes.

5.3.1. Summer and winter maps. We compare in Plate 5 the computed temperature changes in scenarios A, B, and C for June-July-August and December-January-February of the 1990s. In both seasons the warming is much greater in scenario A than in scenarios B and C, as also illustrated

in Figure 3. The relative warmings are consistent with the global radiative forcings for the three scenarios shown in Figure 2; the greater forcing in scenario A arises partly from greater trace gas abundances and partly from the assumed absence of large volcanic eruptions.

Features in the predicted warming common to all scenarios include a tendency for the greatest warming to be in sea ice regions and land areas, as opposed to the open oceans. At high latitudes the warming is greater in winter than in summer. We also notice a tendency for certain patterns in the warming, for example, greater than average warming in the eastern United States and less warming in the western United States. Examination of the changes in sea level pressure and atmospheric winds suggests that this pattern in the model may be related to the ocean's response time; the relatively slow warming of surface waters in the mid Atlantic off the Eastern United States and in the Pacific off California tends to increase sea level pressure in those ocean regions and this in turn tends to cause more southerly winds in the eastern United States and more northerly winds in the western United States. However, the tendency is too small to be apparent every year; in some years in the 1990s the eastern United States is cooler than climatology (the control run mean) and often the western United States is substantially warmer than climatology. Moreover, these regional patterns in the warming could be modified if there were major changes in ocean heat transports.

5.3.2. July maps. We examine in Plate 6 the temperature changes in a single month (July) for several different years of scenario B. In the 1980s the global warming is small compared to the natural variability of local monthly mean temperature; thus any given location is about as likely to be cooler than climatology as warmer than climatology, and, as shown in Plate 6, the area with cool temperatures in a given July is about as great as the area with warm temperatures. But by the year 2000 there is an obvious tendency for it to be warm in more regions, and by the year 2029 it is warm almost everywhere.

Monthly temperature anomalies can be readily noticed by the average person or "man in the street". A calibration of the magnitude of the model predicted warming can be obtained by comparison of Plate 6 with maps of observations for recent years, as published by Hansen *et al.* [1987] using the same color scale as employed here. This comparison shows that the warm events predicted to occur by the 2010s and 2020s are much more severe than those of recent experience, such as the July 1986 heat wave in the southern United States, judging from the area and magnitude of the hot regions.

5.3.3. Frequency of extreme events. Although the greenhouse effect is usually measured by the change of mean temperature, the frequency and severity of extreme temperature events is probably of greater importance to the biosphere. Both plants and animals are affected by extreme temperatures, and regions of habitability are thus often defined by the range of local temperatures.

We estimate the effect of greenhouse warming on the frequency of extreme temperatures by adding the model-predicted warming for a given decade to observed local daily temperatures for the period 1950-1979. This procedure is intended to minimize the effect of errors in the control run

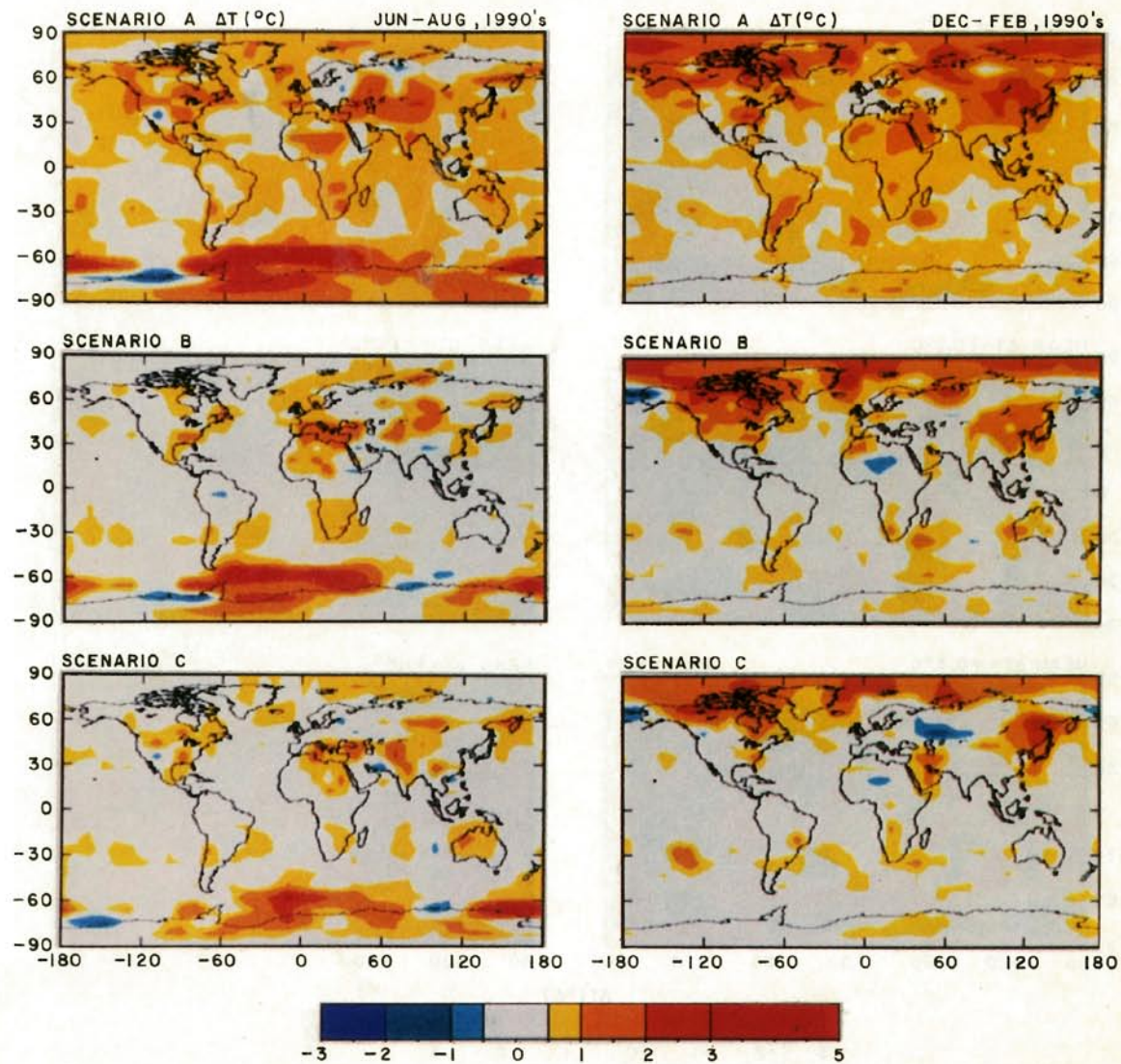


Plate 5. (Left) Simulated June-July-August and (Right) December-January-February temperature anomalies in the 1990s, compared to the 100-year control run with 1958 atmospheric composition.

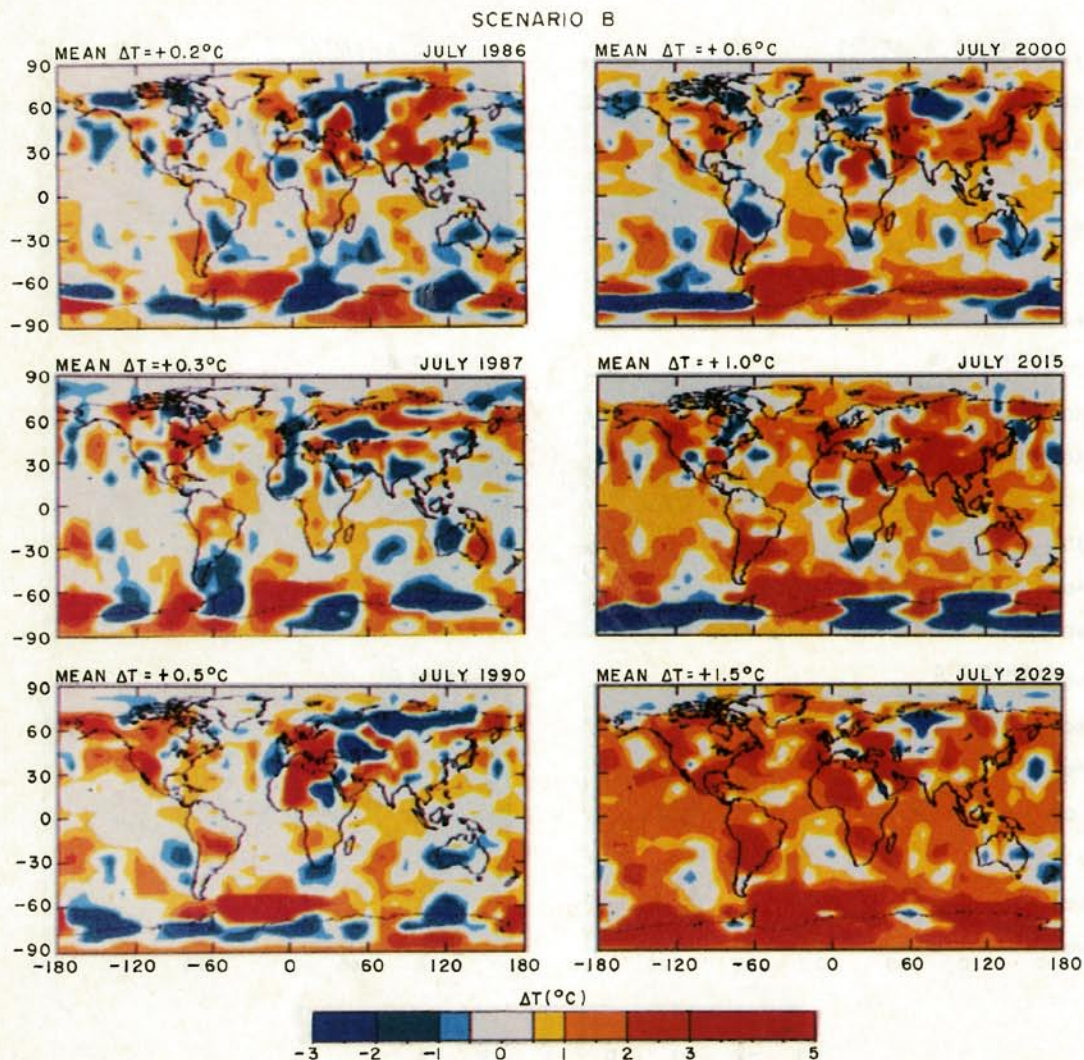


Plate 6. Simulated July surface air temperature anomalies for six individual years of scenario B, compared to the 100-year control run with 1958 atmospheric composition.

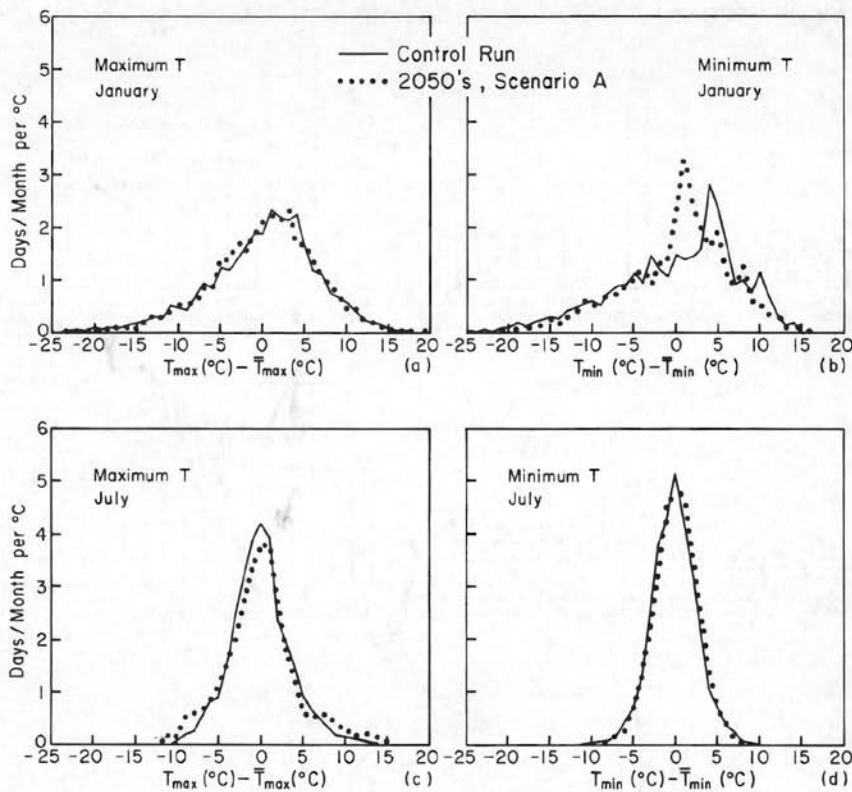


Fig. 4. Distribution of daily maximum and daily minimum temperatures in January and July for 10 grid boxes (latitudes 31° to 47° N, longitudes 75° to 125° W) approximately covering the United States. The solid line represents years 92–100 of the control run and the dotted line is for years 2050–2059 of scenario A. The mean temperature at each grid box is subtracted out first, before computing the mean distribution for the 10 grid boxes.

climatology, which are typically several degrees Centigrade. The principal assumption in this procedure is that the shape of the temperature distribution about the mean will not change much as the greenhouse warming shifts the mean to higher values. We tested this assumption, as shown in Figure 4 for the 10 grid boxes which approximately cover the United States, and found it to be good. The illustrated case is the most extreme in our scenarios, the decade of the 2050s of scenario A, for which the global mean warming is about 4°C . Note in particular that there is no evidence that the distribution toward high temperatures in the summer becomes compressed toward the mean as the mean increases; indeed, the small change in the distribution which occurs is in the sense of greater variability, suggesting that our assumption of no change in the distribution will yield a conservative estimate for the increase in the frequency of hot events.

We also examined the effect of the greenhouse warming on the amplitude of the diurnal cycle of surface air temperature. In our doubled CO_2 experiment [paper 2] the diurnal cycle over land areas decreased by 0.7°C , with greatest changes at low latitudes; for grid boxes in the United States the changes of diurnal amplitude ranged from a decrease of 0.8°C to an increase of 0.5°C . The changes of diurnal amplitude in the transient experiments varied from grid box to grid box, but did not exceed several tenths of a degree centigrade. Thus for simplicity we neglected

this effect in our estimates of changes in the frequencies of extreme temperatures.

The estimated change in the mean number of days per year with temperature exceeding 95°F (35°C), minimum temperature exceeding 75°F ($\approx 24^{\circ}\text{C}$), and minimum temperature below 32°F (0°C) is shown in Figure 5 for several cities. The scenario results were obtained by adding the mean decadal warming (relative to the last 9 years of the control run) of the four model grid points nearest each city to the 1950–1979 observed temperatures. We employ a broad-area 10-year mean change, so that the variability is provided principally by the observed climatology.

The results in Figure 5 illustrate that the predicted changes in the frequency of extreme events in the 1990s generally are less than the observed interannual variability, but the changes become very large within the next few decades. The large effects are not a result of unusual local results in the model's computed ΔT . The computed warmings in the United States are typical of other land areas in the model. For the case of doubled CO_2 , which we can compare with other models, the warming we obtain in the United States (about 4.5°C , see paper 2) is intermediate between the warmings in the GFDL [Manabe and Wetherald, 1987] and NCAR [Washington and Meehl, 1984] models.

Even small temperature changes of less than the interannual variability can be noticeable to the man in the street and can have significant impacts on the bio-

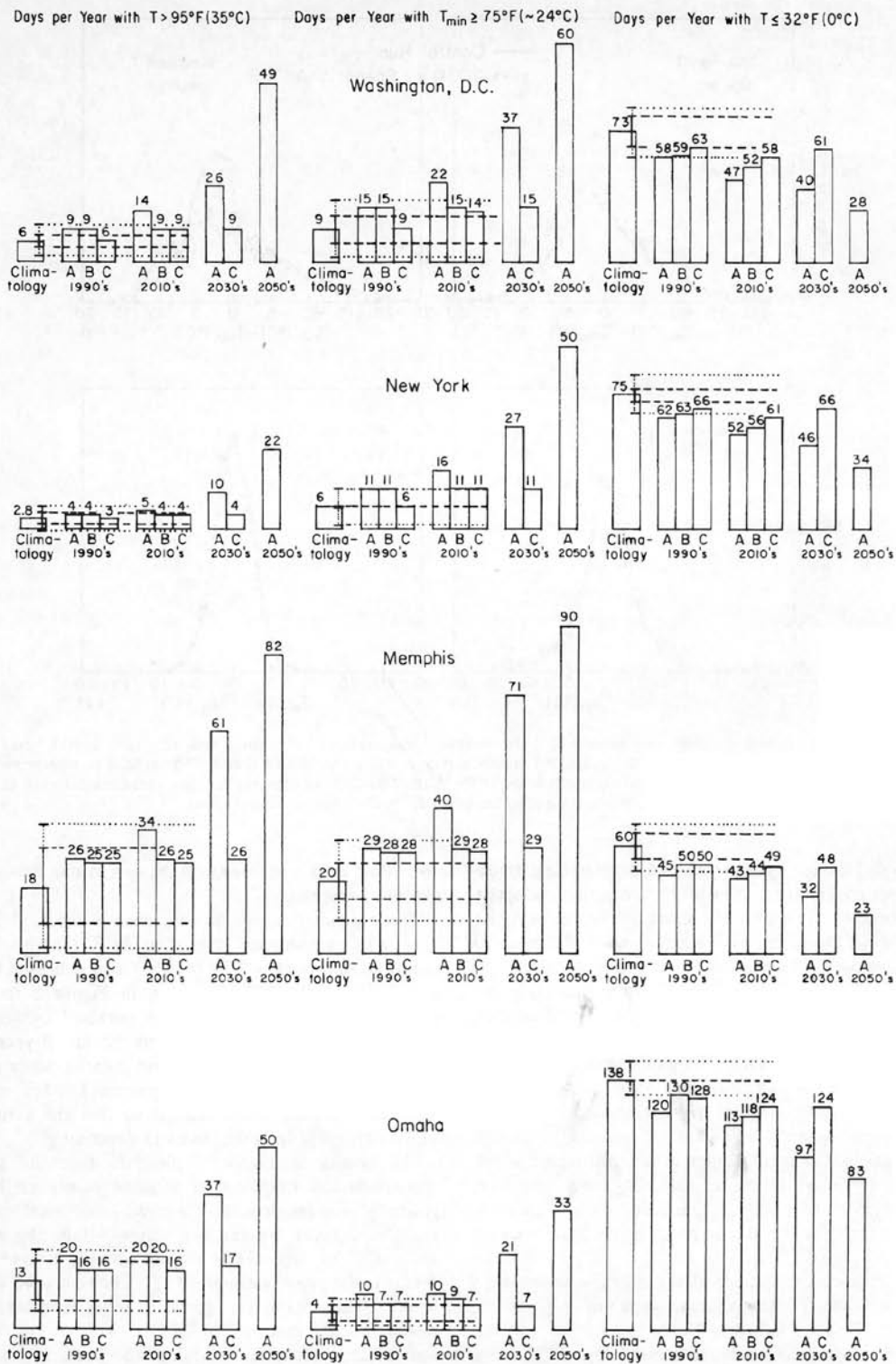


Fig. 5. Climatology and model-based estimates of future frequency of extreme temperature in several cities, specifically: days with maximum temperature above 95°F (35°C), days with minimum temperature above 75°F (~24°C), and days with minimum temperature below 35°F (0°C). Climatology is for the 3 decades 1950–1979; the long and short bars (and the dotted and dashed horizontal lines) specify the interannual and interdecadal variability (standard deviation), respectively, for these 30 years of data. A, B and C represent trace gas scenarios A, B, and C. The vertical scale for days with $T \leq 32°F (0°C)$ is a factor of 2 less than the scale for the other two quantities.

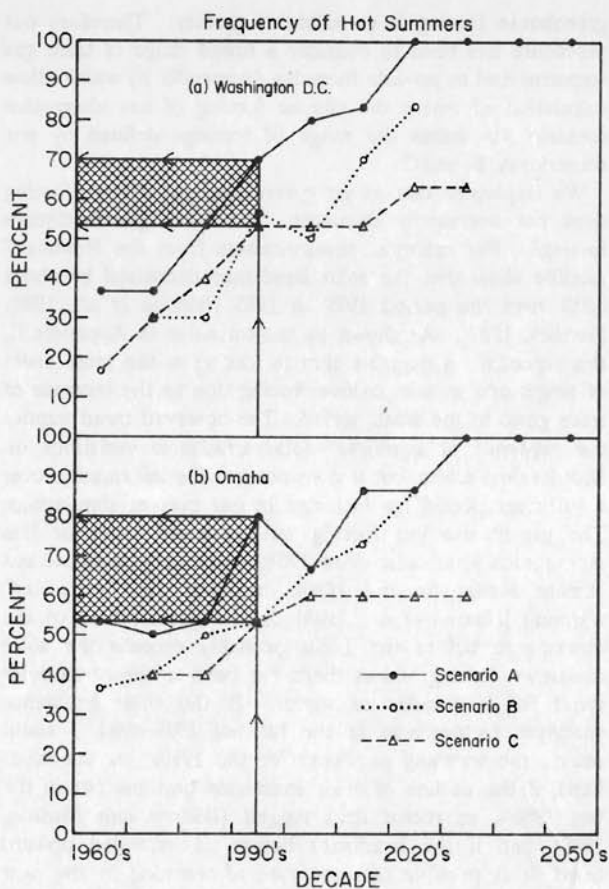


Fig. 6. Estimate of the probability of the summer being "hot", shown for two locations for scenarios A, B, and C. A "hot" summer is one in which the mean temperature exceeds a value which was chosen such that one third of the summers were "hot" in 1950–1979 observations. The estimated probability for hot summers in the 1990s is shown by the shaded region for the range of scenarios.

sphere. As one measure of the detectability of local greenhouse warming, we consider the frequency of warm summers. We arbitrarily define the 10 warmest summers (June–July–August) in the period 1950–1979 as "hot," the 10 coolest as "cold," and the middle 10 as "normal." The impact of the model-computed warming on the frequency of hot summers is illustrated in Figure 6 for the region of Washington, D.C., based on the four grid boxes covering the eastern part of the United States, and for the region of Omaha, based on the four independent west-central grid boxes. In both regions by the 1990s the chance of a hot summer exceeds 50% in all three scenarios, and it exceeds 70% in scenario A.

With hot, normal and cold summers defined by 1950–1979 observations as described earlier, the climatological probability of a hot summer could be represented by two faces (say painted red) of a six-faced die. Judging from our model, by the 1990s three or four of the six die faces will be red. It seems to us that this is a sufficient "loading" of the dice that it will be noticeable to the man in the street. We note, however, that if, say, a blue die face is used for a cold summer, there is still one blue die face in both the

1990s and the first decade of the next century. Thus there remains a substantial likelihood of a cold season at any given location for many years into the future.

We concluded earlier that the magnitude of global mean greenhouse warming should be sufficiently large for scientific identification by the 1990s. We infer from the computed change in the frequency of warm summers that the man in the street is likely to be ready to accept that scientific conclusion. We also conclude that if the world follows a course between scenarios A and B, the temperature changes within several decades will become large enough to have major effects on the quality of life for mankind in many regions.

The computed temperature changes are sufficient to have a large impact on other parts of the biosphere. A warming of 0.5°C per decade implies typically a poleward shift of isotherms by 50 to 75 km per decade. This is an order of magnitude faster than the major climate shifts in the paleoclimate record, and faster than most plants and trees are thought to be capable of naturally migrating [Davis, 1988]. Managed crops will need to be adapted to more extreme conditions in many locales. For example, following the suggestion of S. Schneider (private communication, 1987) we estimated the effect of greenhouse warming on the likelihood of a run of 5 consecutive days with maximum temperature above 95°F . Observations at Omaha, Nebraska for the 30-year period 1950–1979 show 3 years per decade with at least one such run of 95°F temperatures. With the warming from our model this becomes 5 years per decade in the 1990s in scenario A (4 years per decade in scenarios B and C), 7 years per decade in the 2020s in scenario A (6 years per decade in scenario B and 4 years per decade in scenario C), and 9 years per decade for doubled CO_2 . Such temperature extremes are thought to be harmful to corn productivity [Means et al., 1984]; thus these results imply that the impact on crops can be very nonlinear with increasing mean temperature. Another example of nonlinear response by the biosphere to increasing temperature is evidence that many coral populations expell their symbiotic algae when water temperature rises above about 30°C , which leads to death of the coral if temperatures remain in that range, as evidenced by recent events in the tropics [Roberts, 1987].

Negative impacts of greenhouse warming on the biosphere are undoubtedly greatest in regions where species are close to maximum temperature tolerance limits. Such impacts may be at least partially balanced by improved opportunities for productive life in other regions. Also the "fertilization" effect on crops due to increasing atmospheric CO_2 [Lemon, 1983] and other greenhouse climate effects such as changes in precipitation [Manabe and Wetherald, 1987] may have impacts besides that of the temperature change. Our intention here is only to show that temperature changes themselves can have a major impact on life and that these effects may begin to be felt soon. We emphasize that it is the possibility of rapid climate change which is of most concern for the biosphere; there may not be sufficient time for many ecosystems to adapt to the rapid changes forecast for scenarios A and B.

6. DISCUSSION

Our simulations of the global climate response to realistic time-dependent changes of atmospheric trace gases and

aerosols yield the following results: (1) global warming within the next few decades at least to the maximum levels achieved during the last few interglacial periods occurs for all the trace gas scenarios which we consider, but the magnitude of further warming depends greatly on future trace gas growth rates; (2) the global greenhouse warming should rise above the level of natural climate variability within the next several years, and by the 1990s there should be a noticeable increase in the local frequency of warm events; (3) some regions where the warming should be apparent earliest are low-latitude oceans, certain continental areas, and sea ice regions; the three-dimensional pattern of the predicted warming is model-dependent, implying that appropriate observations can provide discrimination among alternative model representations and thus lead to improved climate predictions; (4) the temperature changes are sufficiently large to have major impacts on man and his environment, as shown by computed changes in the frequency of extreme events and by comparison with previous climate trends; (5) some near-term regional climate variations are suggested; for example, there is a tendency in the model for greater than average warming in the southeastern and central United States and relatively cooler conditions or less than average warming in the western U.S. and much of Europe in the late 1980s and in the 1990s.

In this section we summarize the principal assumptions upon which these results depend. In the subsection 6.5 we stress the need for global observations and the development of more realistic models.

6.1. Climate Sensitivity

The climate model we employ has a global mean surface air equilibrium sensitivity of 4.2°C for doubled CO_2 . Other recent GCMs yield equilibrium sensitivities of $2.5^{\circ}\text{--}5.5^{\circ}\text{C}$, and we have presented empirical evidence favoring the range $2.5^{\circ}\text{--}5^{\circ}\text{C}$ (*paper 2*). Reviews by the National Academy of Sciences [Charney, 1979; Smagorinsky, 1982] recommended the range $1.5^{\circ}\text{--}4.5^{\circ}\text{C}$, while a more recent review by Dickinson [1986] recommended $1.5^{\circ}\text{--}5.5^{\circ}\text{C}$.

Forecast temperature trends for time scales of a few decades or less are not very sensitive to the model's equilibrium climate sensitivity [Hansen et al., 1985]. Therefore climate sensitivity would have to be much smaller than 4.2°C , say $1.5\text{--}2^{\circ}\text{C}$, in order to modify our conclusions significantly. Although we have argued [*paper 2*] that such a small sensitivity is unlikely, it would be useful for the sake of comparison to have GCM simulations analogous to the ones we presented here, but with a low climate sensitivity. Until such a study is completed, we can only state that the observed global temperature trend is consistent with the "high" climate sensitivity of the present model. However, extraction of the potential empirical information on climate sensitivity will require observations to reduce other uncertainties, as described below. The needed observations include other climate forcings and key climate processes such as the rate of heat storage in the ocean.

6.2. Climate Forcings

Climate forcing due to increasing atmospheric greenhouse gases in the period from 1958 to the present is uncertain by perhaps 20% (Appendix B); the uncertainty about future

greenhouse forcing is considerably greater. Therefore our procedure has been to consider a broad range of trace gas scenarios and to provide formulae (Appendix B) which allow calculation of where the climate forcing of any alternative scenario fits within the range of forcings defined by our scenarios A, B, and C.

We emphasize that as yet greenhouse gas climate forcing does not necessarily dominate over other global climate forcings. For example, measurements from the Nimbus 7 satellite show that the solar irradiance decreased by about 0.1% over the period 1979 to 1985 [Willson et al., 1986; Fröhlich, 1987]. As shown by the formulae in Appendix B, this represents a negative climate forcing of the same order of magnitude as the positive forcing due to the increase of trace gases in the same period. The observed trend implies the existence of significant solar irradiance variations on decadal time scales, but it does not provide information over a sufficient period for inclusion in our present simulations. The greenhouse gas forcing has increased more or less monotonically, at least since 1958; thus the greenhouse gas climate forcing in the 1980s including the "unrealized" warming [Hansen et al., 1985] due to gases added to the atmosphere before the 1980s probably exceeds the solar irradiance forcing, unless there has been a consistent solar trend for 2 decades or more. If the solar irradiance continues to decrease at the rate of 1979–1985 it could reduce the warming predicted for the 1990s; on the other hand, if the decline of solar irradiance bottoms out in the late 1980's, as recent data suggest [Willson and Hudson, 1988], and if the irradiance begins an extended upward trend, it is possible that the rate of warming in the next decade could exceed that in our present scenarios. Continued monitoring of the solar irradiance is essential for interpretation of near-term climate change and early identification of greenhouse warming.

Stratospheric aerosols also provide a significant global climate forcing, as evidenced by the effects of Mt. Agung (1963) and El Chichón (1982) aerosols on our computed global temperatures. Thus if a very large volcanic eruption occurred in the next few years, it could significantly reduce the projected warming trend for several years. On the other hand, if there are no major volcanic eruptions in the remainder of the 1980s or the 1990s, that would tend to favor more rapid warming than obtained in scenarios B and C, which assumed an eruption in the mid-1990s of the magnitude of El Chichón. Interpretation of near-term climate change will require monitoring of stratospheric aerosols, as well as solar irradiance.

Other climate forcings, such as changes in tropospheric aerosols or surface albedo, are also potentially significant (Appendix B); they probably are important on a regional basis, and perhaps influence the temperature of the entire northern hemisphere. Examples of changing aerosol abundance include the arctic haze, long-range transport of desert aerosols, and perhaps urban and rural aerosols of anthropogenic origin. Significant surface albedo variations may be associated with large-scale deforestation and desertification, but available information on trends is not sufficiently quantitative for inclusion in our global simulations. It is desirable that calibrated long-term monitoring of tropospheric aerosols and surface albedo be obtained in the future.

6.3. Ocean Heat Storage and Transport

Our ocean model is based on the assumption that for the small climate forcings of the past few decades and the next few decades, horizontal transport of heat by the ocean will not change significantly and uptake of heat perturbations by the ocean beneath the mixed layer will be at a rate similar to that of passive tracers simulated as a diffusive process. We believe that these assumptions give a global result which is as reliable as presently possible, given available knowledge and modeling abilities for the ocean; in any case, this approach provides a first result against which later results obtained with dynamically interactive oceans can be compared.

However, we stress that our ocean model yields relatively smooth surprise-free temperature trends. It excludes the possibility of shifts in ocean circulation or in the rate of deepwater formation. There is evidence in paleoclimate records that such ocean fluctuations have occurred in the past [Broecker et al., 1985], especially in the North Atlantic, where, for example, a reduction in the rate of deepwater formation could reduce the strength of the Gulf Stream and thus lead to a cooling in Europe. We caution that our ocean model assumptions exclude the possibility of such sudden shifts in regional or global climate.

We also stress the importance of measuring the rate of heat storage in the ocean. As discussed earlier and by Hansen et al. [1985], on the time scale of a few decades there is not necessarily a great difference in the surface temperature response for a low climate sensitivity (say 1.5°–2°C for doubled CO₂) and a high climate sensitivity (say 4°–5°C for doubled CO₂). However, the larger climate sensitivity leads to a higher rate of heat storage in the ocean. Since theoretical derivations of climate sensitivity depend so sensitively on many possible climate feedbacks, such as cloud and aerosol optical properties [Somerville and Remer, 1984; Charlson et al., 1987], the best opportunity for major improvement in our understanding of climate sensitivity is probably monitoring of internal ocean temperature. Such measurements would be needed along several sections crossing the major oceans. In principle, the measurements would only be needed at decadal intervals, but continuous measurements are highly desirable to average out the effect of local fluctuations.

6.4. Initial Conditions

Because of the long response time of the ocean surface temperature, the global surface temperature can be in substantial disequilibrium with the climate forcing at any given time. By initiating our experiments in 1958 after a long control run with 1958 atmospheric composition, we implicitly assume that the ocean temperature was approximately in equilibrium with the initial atmospheric composition. Our results could be significantly modified by a different assumption. For example, if there were substantial unrealized greenhouse warming in 1958 due to a steady increase of greenhouse forcing between the 1800s and 1958, incorporation of that disequilibrium in our initial conditions would have caused the global temperature to rise faster than it did in our experiments. We initiated our experiments in 1958 principally because that is when accurate CO₂ measurements began. However, 1958 also appears to be a good starting point to minimize the possibility of a major dis-

equilibrium between the initial ocean surface temperature and the atmospheric forcing. Global temperature peaked about 1940 and was level or declined slightly in the 2 decades between 1940 and 1958. Regardless of whether the 1940 maximum was an unforced fluctuation of temperature or due to a maximum of some climate forcing, one effect of that warm period is to reduce and perhaps eliminate any unrealized greenhouse warming in 1958.

It would be useful to also carry out simulations which begin in say the 1800s, thus reducing uncertainties due to possible disequilibrium in the initial conditions. These experiments would be particularly appropriate for extracting empirical information on climate sensitivity from the observed warming in the past century. Such experiments were beyond the capability of our computer (circa 1975 Amdahl). Moreover, because of greater uncertainties in climate forcings before 1958, such experiments probably would not yield more reliable predictions of future climate trends.

6.5. Summary

Our model results suggest that global greenhouse warming will soon rise above the level of natural climate variability. The single best place to search for the greenhouse effect appears to be the global mean surface air temperature. If it rises and remains for a few years above an appropriate significance level, which we have argued is about 0.4°C for 99% confidence (3σ), it will constitute convincing evidence of a cause and effect relationship, i.e., a "smoking gun," in current vernacular.

Confirmation of the global warming will enhance the urgency of innumerable questions about the practical impacts of future climate change. Answers to these questions will depend upon the details of the timing, the magnitude and the global distribution of the changes of many climate parameters, information of a specificity which cannot presently be provided. Major improvements are needed in our understanding of the climate system and our ability to predict climate change.

We conclude that there is an urgent need for global measurements in order to improve knowledge of climate forcing mechanisms and climate feedback processes. The expected climate changes in the 1990s present at once a great scientific opportunity, because they will provide a chance to discriminate among alternative model representations, and a great scientific challenge, because of demands that will be generated for improved climate assessment and prediction.

APPENDIX A: OCEAN MODEL AND OCEAN DATA

The seasonal transport of heat in our ocean model is specified by the convergence (or divergence) of heat at each ocean grid point, determined from energy balance as the difference between the time rate of change of heat storage and the heat flux at the air sea interface. The heat storage is calculated from the Robinson and Bauer [1981] ocean surface temperatures, the northern hemisphere horizontal ice extent of Walsh and Johnson [1979], the southern hemisphere ice extent of Alexander and Mobley [1974], and mixed layer depths compiled from National Oceanographic Data Center (NODC) bathythermograph data [National Oceanic and Atmospheric Administration (NOAA),

1974]. The surface heat flux was saved from a 2 year run of model II (*paper 1*) which used these monthly ocean surface temperatures as boundary conditions. Figure 1 of paper 2 shows this surface heat flux. The calculation of the ocean heat transport is described in more detail by *Russell et al.* [1985], whose Figure 5 shows the geographical distribution of the mixed layer depths for February and August. The global area-weighted value of the annual maximum mixed layer depth is 127 m.

The gross characteristics of the ocean surface heat flux and implied ocean heat transport appear to be realistic, with heat gain and flux divergence at low latitudes and heat loss and flux convergence at high latitudes. A comprehensive comparison of the annual ocean heat transport by *Miller et al.* [1983] shows that the longitudinally integrated transport in each ocean basin is consistent with available knowledge of actual transports.

In our 100-year control run there is no exchange of heat at the base of the mixed layer. In the experiments with varying atmospheric composition, we mimic, as a diffusion process, the flux of temperature anomalies from the mixed layer into the thermocline. The thermocline, taken to be the water below the annual maximum mixed layer, is structured with eight layers of geometrically increasing thickness, with a total thickness of about 1000 m.

An effective diffusion coefficient, k , is estimated below the annual maximum mixed layer of each grid point using an empirical relation between the penetration of transient inert tracers and the local water column stability (*paper 2*), the latter being obtained from the annual mean density distribution calculated from *Levitus* [1982]. The resulting global distribution of k is shown in Figure 15a of paper 2. There is a low exchange rate ($k \approx 0.2 \text{ cm}^2 \text{s}^{-1}$) at low latitudes and a high exchange rate in the North Atlantic and southern oceans, where convective overturning occurs. Note that k is constant in time and in the vertical direction.

The ocean temperature and the ocean ice state in the transient experiments are computed based on energy balance. The specified converged ocean heat and the diffusion into the thermocline are deposited into or removed from the active mixed layer. The surface flux heats (or cools) the open ocean and ocean ice in proportion to their exposed areas. In addition, there is a vertical exchange (conduction) of heat between the ocean and the ice above it.

When the surface fluxes would cool the mixed layer below -1.6°C , the mixed layer stays at -1.6°C and ice with 1-m thickness is formed, growing horizontally at a rate determined by energy balance. When the surface fluxes would warm the ocean above 0°C , the ocean stays at 0°C until all ice in the grid box is melted horizontally. Conductive cooling at the ice/water interface thickens the ice if the ocean temperature is at -1.6°C . Leads are crudely represented by requiring that the fraction of open water in a grid box not be less than $0.1/z_{\text{ice}}$, where z_{ice} is the ice thickness in meters (*paper 1*).

APPENDIX B: RADIATIVE FORCINGS

Radiative forcing of the climate system can be specified by the global surface air temperature change ΔT_o that would be required to maintain energy balance with space if no climate feedbacks occurred (*paper 2*). Radiative forcings for a variety of changes of climate boundary conditions are

compared in Figure B1, based on calculations with a one-dimensional radiative-convective (RC) model [*Lacis et al.*, 1981]. The following formulas approximate the ΔT_o from the 1D RC model within about 1% for the indicated ranges of composition. The absolute accuracy of these forcings is of the order of 10% because of uncertainties in the absorption coefficients and approximations in the 1D calculations.

CO_2

$$\begin{aligned}\Delta T_o(x) &= f(x) - f(x_0); \\ f(x) &= \ln(1 + 1.2x + 0.005x^2 + 1.4 \times 10^{-6}x^3); \\ x_0 &= 315 \text{ ppmv}, \quad x \leq 1000 \text{ ppmv}\end{aligned}$$

CCl_2F_2

$$\Delta T_o(x) = 0.084(x - x_0); \quad x - x_0 \leq 2 \text{ ppbv}$$

CCl_3F

$$\Delta T_o(x) = 0.066(x - x_0); \quad x - x_0 \leq 2 \text{ ppbv}$$

CH_4

$$\Delta T_o = g(x, y_o) - g(x_o, y_o); \quad x, x_o \leq 5 \text{ ppmv}$$

N_2O

$$\Delta T_o = g(x_o, y) - g(x_o, y_o); \quad y, y_o \leq 5 \text{ ppmv}$$

where, for CH_4 and N_2O , x_o , y_o are reference amounts, respectively, and

$$\begin{aligned}g(x, y) &= \frac{0.394x^{0.66} + 0.16x \exp(-1.6x)}{1 + 0.169x^{0.62}} \\ &\quad + 1.556 \ln \left[1 + y^{0.77} \frac{109.8 + 3.5y}{100 + 0.14y^2} \right] \\ &\quad - 0.014 \ln [1 + 0.636(xy)^{0.75} + 0.007x(xy)^{1.52}];\end{aligned}$$

H_2SO_4 aerosols (20 km)

$$\Delta T_o(\tau) = -5.8\tau; \quad \tau (\lambda = 550 \text{ nm}) \leq 0.2$$

H_2SO_4 aerosols (0-2km)

$$\Delta T_o(\tau) = -6.5\tau; \quad \tau (\lambda = 550 \text{ nm}) \leq 0.2$$

Solar irradiance

$$\Delta T_o(x) = 0.67x; \quad x = \Delta S_o(\%) \leq 1\%$$

Land albedo

$$\Delta T_o(x) = -0.12x; \quad x = \Delta \text{albedo of land area} \leq 0.1$$

Trace gas scenarios. Trace gas trends beginning in 1958 (when accurate measurements of CO_2 began) were estimated from measurement data available in early 1983, when we initiated our transient simulations. References to the measurements are given by *Shands and Hoffman* [1987]. Figure B2 summarizes the estimated decadal increments to global greenhouse forcing. The forcings shown by dotted lines in Figure B2 are speculative; their effect was included in scenario A but was excluded in scenarios B and C. The CH_4 forcing in the 1980s represents a $1.5\% \text{ yr}^{-1}$ growth rate; recent data [*Bolle et al.*, 1986, *Blake and Rowland*, 1987] suggest that a $1.1\% \text{ yr}^{-1}$ growth rate probably is more realistic.

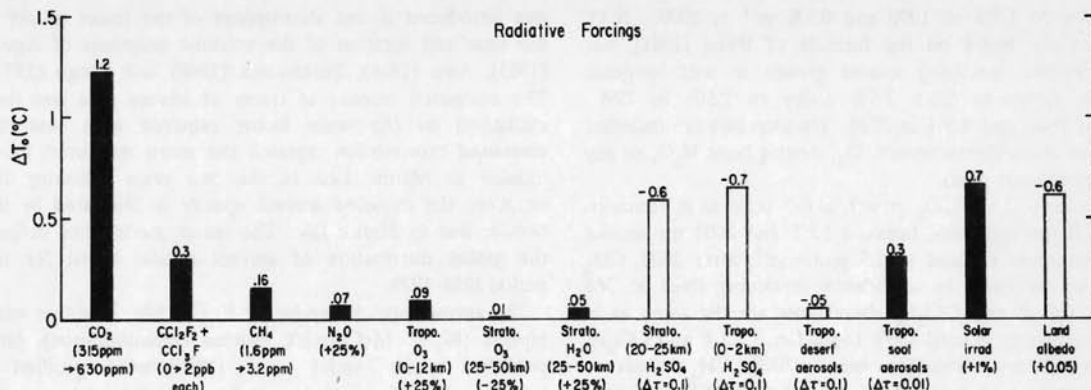


Fig. B1. Global mean radiative forcing of the climate system for arbitrary changes of radiative parameters. Here ΔT_0 is the temperature change at equilibrium ($t \rightarrow \infty$) computed with a 1D RC model for the specified change in radiative forcing parameter with no climate feedbacks included; ΔT_0 must be multiplied by a feedback factor f to get the equilibrium surface temperature change including feedback effects (paper 2). Tropospheric aerosols are all placed in the lower 2 km of the atmosphere; the desert aerosols have effective radius $r_{\text{eff}} \approx 2 \mu\text{m}$ and single scattering albedo $\omega \approx 0.8$ at wavelength $\lambda = 550 \text{ nm}$, while the soot aerosols have $r_{\text{eff}} \approx 1 \mu\text{m}$ and $\omega \approx 0.5$. The land albedo change of 0.05 is implemented via a change of 0.015 in the surface albedo, corresponding to 30% land cover.

Specifically, in scenario A CO_2 increases as observed by Keeling for the interval 1958–1981 [Keeling et al., 1982] and subsequently with $1.5\% \text{ yr}^{-1}$ growth of the annual increment. CCl_3F (F-11) and CCl_2F_2 (F-12) emissions are from reported rates [Chemical Manufacturers Association (CMA) 1982] and assume $3\% \text{ yr}^{-1}$ increased emission in the future, with atmospheric lifetimes for the gases of 75 and 150 years, respectively. CH_4 , based on estimates given by Laca et al. [1981], increases from 1.4 ppbv in 1958 at a rate of $0.6\% \text{ yr}^{-1}$ until 1970, $1\% \text{ yr}^{-1}$ in the 1970s and $1.5\% \text{ yr}^{-1}$ thereafter. N_2O increases according to the semiempirical formula of Weiss [1981], the rate being $0.1\% \text{ yr}$ in 1958, 0.2%

yr^{-1} in 1980, $0.4\% \text{ yr}^{-1}$ in 2000, and $0.9\% \text{ yr}^{-1}$ in 2030. Potential effects of several other trace gases (such as O_3 , stratospheric H_2O , and chlorine and fluorine compounds other than CCl_3F and CCl_2F_2) are approximated by multiplying the CCl_3F and CCl_2F_2 amounts by 2.

In scenario B the growth of the annual increment of CO_2 is reduced from $1.5\% \text{ yr}^{-1}$ today to $1\% \text{ yr}^{-1}$ in 1990, $0.5\% \text{ yr}^{-1}$ in 2000, and 0 in 2010; thus after 2010 the annual increment in CO_2 is constant, 1.9 ppmv yr^{-1} . The annual growth of CCl_3F and CCl_2F_2 emissions is reduced from $3\% \text{ yr}^{-1}$ today to $2\% \text{ yr}^{-1}$ in 1990, $1\% \text{ yr}^{-1}$ in 2000 and 0 in 2010. The methane annual growth rate decreases from 1.5%

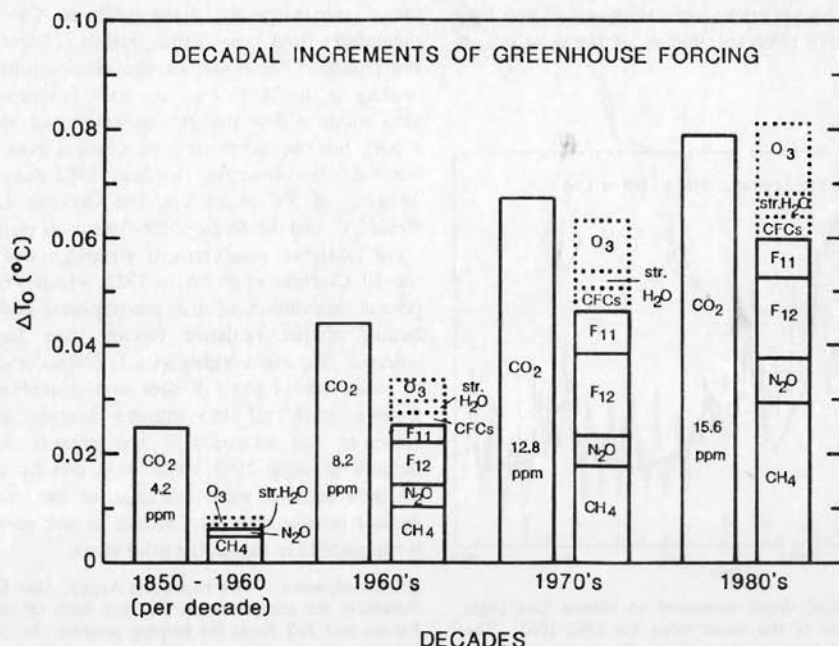


Fig. B2. Estimated decadal additions to global mean greenhouse forcing of the climate system. The value of ΔT_0 is defined in the caption of Figure B1. Forcings shown by dotted lines are highly speculative.

yr^{-1} today to 1.0% in 1990 and 0.5% yr^{-1} in 2000. N_2O increases are based on the formula of Weiss [1981], but the parameter specifying annual growth in anthropogenic emission decreases from 3.5% today to 2.5% in 1990, 1.5% in 2000, and 0.5% in 2010. No increases are included for other chlorofluorocarbons, O_3 , stratospheric H_2O , or any other greenhouse gases.

In scenario C the CO_2 growth is the same as in scenarios A and B through 1985; between 1985 and 2000 the annual CO_2 increment is fixed at 1.5 ppmv yr^{-1} ; after 2000, CO_2 ceases to increase, its abundance remaining fixed at 368 ppmv. CCl_3F and CCl_2F_2 abundances are the same as in scenarios A and B until 1990; thereafter, CCl_3F and CCl_2F_2 emissions decrease linearly to zero in 2000. CH_4 abundance is the same as in scenarios A and B until 1980; between 1980 and 1990 its growth rate is 1% yr^{-1} ; between 1990 and 2000 its growth rate is 0.5% yr^{-1} ; after 2000, CH_4 ceases to increase, its abundance remaining fixed at 1916 ppbv. As in scenario B, no increases occur for the other chlorofluorocarbons, O_3 , stratospheric H_2O , or any other greenhouse gases.

Stratospheric aerosol scenarios. The radiative forcing due to stratospheric aerosols depends principally upon their optical thickness at visible wavelengths, their opacity in the thermal infrared region, and their global distribution. Because of the small size of long-lived stratospheric aerosols, their effect on planetary albedo generally exceeds their effect on infrared transmission [Hansen et al., 1980]. Thus the most important aerosol radiative parameter is the optical thickness at visible wavelengths, τ . We base the estimated τ before El Chichón primarily on solar transmission measurements at Mauna Loa [Mendonca, 1979], together with calculations with a 3D tracer model [Russell and Lemer, 1981].

The measured optical depth at Mauna Loa, after subtraction of the mean 1958–1962 value, which is assumed to represent the local background value, is shown as the light line in Figure B3. An arbitrary amount of tracer substance

was introduced in the stratosphere of the tracer model at the time and location of the volcanic eruptions of Agung (1963), Awu (1966), Fernandina (1968) and Fuego (1974). The computed amount of tracer at Mauna Loa was then multiplied by the scale factor required such that the computed transmission equaled the mean measured transmission at Mauna Loa in the two years following the eruption; the modeled aerosol opacity is illustrated by the heavier line in Figure B3. The tracer model thus defined the global distribution of aerosol optical depth for the period 1958–1979.

The aerosol optical depths for El Chichón, based on early reports (M. P. McCormick, private communication), later published by McCormick et al., [1984], were specified as follows. For the first 6 months after the eruption, the opacity was uniformly distributed between the equator and 30°N, increasing linearly from $\tau=0$ at the time of eruption to $\tau=0.25$ 3 months after the eruption and remaining constant for the next 3 months. Subsequently, the opacity was uniform from 90° to 30°N and from 30°N to 90°S, but with 2 times greater τ in the northern region than in the southern region. Beginning 10 months after the eruption, τ decayed exponentially with a 12-month time constant.

The optical properties of the stratospheric aerosols before 1982 are based on measurements of Agung aerosols. The size distribution we used is that given by Toon and Pollack [1976], which is based on measurements by Mossop [1964]; it has mean effective radius and variance [Hansen and Travis, 1974] of $r_{\text{eff}} \approx 0.2 \mu\text{m}$ and $v_{\text{eff}} \approx 0.6$. These aerosols are assumed to be spheres of sulfuric acid solution (75% acid by weight) with refractive index given by Palmer and Williams [1975]. We used size data for the El Chichón aerosols based on measurements of Hoffman and Rosen [1983]. Their May 1982 data had $r_{\text{eff}} \approx 1.4 \mu\text{m}$, $v_{\text{eff}} \approx 0.4$, while their October 1982 data had $r_{\text{eff}} \approx 0.5 \mu\text{m}$, $v_{\text{eff}} \approx 0.15$. We interpolated linearly between these two size distributions for the 6 month period April 1982 to October 1982, and thereafter used the small-particle (October 1982) size distribution. These various size distributions yield the same cooling at the Earth's surface as a function of τ ($\lambda = 550 \text{ nm}$) within a few percent, as computed with the 1D RC model, but the large particles cause a greater stratospheric heating. For example, the May 1982 distribution yields a warming of 5°C at 23 km, the October 1982 distribution yields 2°C, and the Mossop [1964] aerosols yield 1.5°C.

An extensive measurement campaign was mounted after the El Chichón eruption in 1982, which will allow a more precise calculation of the geographical and altitude distribution of the radiative forcing than for any previous volcano. We are working with J. Pollack and P. McCormick to make use of the full data now available for a comprehensive study of the climate impact in that period. However, the scenarios in our present simulations were defined in early 1983 when only sketchy data on the El Chichón aerosols were available, so the uncertainty in the aerosol forcing after El Chichón in our present simulations is comparable to that in the prior years.

Acknowledgments. We thank Jim Angell, Alan Robock and Steve Schneider for comments on the first draft of this paper, Patrice Palmer and Jeff Jonas for helping produce the color figures, Jose Mendoza for drafting other figures, and Carolyn Paurowski for desktop typesetting. This work has been supported by the NASA Climate Program and EPA grant R812962-01-0.

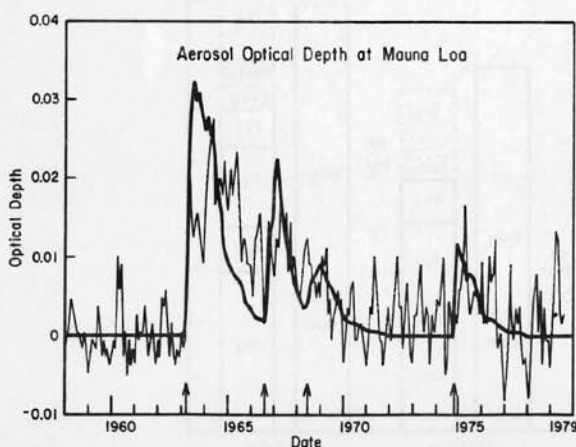


Fig. B3. Aerosol optical depth measured at Mauna Loa (light curve) after subtraction of the mean value for 1958–1962. The heavy line is the optical depth at Mauna Loa, obtained from the 3D tracer model, as discussed in the text. The arrows mark the times of eruption of Agung, Awu, Fernandina and Fuego, respectively.

REFERENCES

- Alexander, R. C., and R. L. Mobley, Monthly average sea-surface temperature and ice-pack limits on a 1° global grid, *Rep. 4-1310-ARPA*, 30 pp., Rand Corp., Santa Monica, 1974.
- Angell, J. K., Annual and seasonal global temperature changes in the troposphere and low stratosphere, 1960–1985, *Mon. Weather Rev.*, **114**, 1922–1930, 1986.
- Barnett, T. P., Detection of changes in the global troposphere temperature field induced by greenhouse gases, *J. Geophys. Res.*, **91**, 6659–6667, 1986.
- Bell, T. L., Optimal weighting of data to detect climate change: Application to the carbon dioxide problem, *J. Geophys. Res.*, **87**, 11, 161–11,170, 1982.
- Blake, D. and S. Rowland, Increasing global concentrations of tropospheric methane, paper presented at Symposium on Atmospheric Methane, Am. Chem. Soc., Denver, Colo., April 5–10, 1987.
- Bolle, H. J., W. Seiler, and B. Bolin, Other greenhouse gases and aerosols, in *The Greenhouse Effect, Climate Change, and Ecosystems*, edited by B. Bolin, B. A. Doos, J. Jager and R. A. Warrick, pp. 157–203, John Wiley, New York, 1986.
- Broecker, W. S., D. M. Peteet, and D. Rind, Does the ocean-atmosphere system have more than one stable mode of operation?, *Nature*, **315**, 21–26, 1985.
- Bryan, K., F. G. Komro, and C. Rooth, The ocean's transient response to global surface temperature anomalies, in *Climate Processes and Climate Sensitivity*, *Geophys. Monogr. Ser.*, Vol. 29, edited by J. E. Hansen and T. Takahashi, pp. 29–38, AGU, Washington D.C., 1984.
- Charlson, R. J., J. E. Lovelock, M. O. Andreae, and S. G. Warren, Oceanic phytoplankton, atmospheric sulphur, cloud albedo and climate, *Nature*, **326**, 655–661, 1987.
- Charney, J., Carbon dioxide and climate: A scientific assessment, 33 pp., National Academy Press, Washington, D.C., 1979.
- Chemical Manufacturers Association, World production and release of chlorofluorocarbons 11 and 12 through 1981, Calculations by E. I. du Pont de Nemours and Company, Inc., Washington, D.C., 1982.
- Davis, M. B., Lags in vegetation response to climate change, *Clim. Change*, in press, 1988.
- Dickinson, R. E., The climate system and modeling of future climate, in *The Greenhouse Effect, Climate Change, and Ecosystems*, edited by B. Bolin, B. A. Doos, J. Jager, and R. A. Warrick, pp. 206–270, John Wiley, New York, 1986.
- Frohlich, C., Variability of the solar "constant" on time scales of minutes to years, *J. Geophys. Res.*, **92**, 796–800, 1987.
- Hansen, J., and S. Lebedeff, Global trends of measured surface air temperature, *J. Geophys. Res.*, **92**, 13,345–13,372, 1987.
- Hansen, J., and S. Lebedeff, Global surface air temperatures: update through 1987, *Geophys. Res. Lett.*, **15**, 323–326, 1988.
- Hansen, J. E., and L. D. Travis, Light scattering in planetary atmospheres, *Space Sci. Rev.*, **16**, 527–610, 1974.
- Hansen, J. E., W. C. Wang, and A. A. Lacis, Mount Agung eruption provides test of a global climatic perturbation, *Science*, **199**, 1065–1068, 1978.
- Hansen, J. E., A. A. Lacis, P. Lee, and W. C. Wang, Climatic effects of atmospheric aerosols, *Ann. N. Y. Acad. Sci.*, **338**, 575–587, 1980.
- Hansen, J., E. Johnson, A. Lacis, S. Lebedeff, P. Lee, D. Rind, and G. Russell, Climate impact of increasing atmospheric carbon dioxide, *Science*, **213**, 957–966, 1981.
- Hansen, J., G. Russell, D. Rind, P. Stone, A. Lacis, S. Lebedeff, R. Ruedy and L. Travis, Efficient three-dimensional global models for climate studies: models I and II, *Mon. Weather Rev.*, **111**, 609–662, 1983.
- Hansen, J., A. Lacis, D. Rind, G. Russell, P. Stone, I. Fung, R. Ruedy, and J. Lerner, Climate sensitivity: Analysis of feedback mechanisms, in *Climate Processes and Climate Sensitivity*, *Geophys. Monogr. Ser.*, Vol. 29, edited by J. E. Hansen and T. Takahashi, pp. 130–163, AGU, Washington, D.C., 1984.
- Hansen, J., G. Russell, A. Lacis, I. Fung, D. Rind, and P. Stone, Climate response times: Dependence on climate sensitivity and ocean mixing, *Science*, **229**, 857–859, 1985.
- Hansen, J., I. Fung, A. Lacis, S. Lebedeff, D. Rind, R. Ruedy, and G. Russell, Predictions of near-term climate evolution: What can we tell decision makers now?, paper presented at First North American Conference on Preparing for Climate Change, Climate Institute, Washington, Oct. 27–29, 1987.
- Hasselmann, K., Stochastic climate models, I. Theory, *Tellus*, **28**, 473–485, 1976.
- Hoffman, D. J., and J. M. Rosen, Sulfuric acid droplet formation and growth in the stratosphere after the 1982 eruption of El Chichón, *Science*, **222**, 325–327, 1983.
- Keeling, C. D., R. B. Bacastow, and T. P. Whorf, Measurements of the concentration of carbon dioxide at Mauna Loa observatory, Hawaii, in *Carbon Dioxide Review: 1982*, edited by W. C. Clark, pp. 377–385, Oxford University Press, New York, 1982.
- Lacis, A., J. Hansen, P. Lee, T. Mitchell and S. Lebedeff, Greenhouse effect of trace gases, 1970–1980, *Geophys. Res. Lett.*, **8**, 1035–1038, 1981.
- Lamb, H. H., Volcanic dust in the atmosphere: With a chronology and assessment of its meteorological significance, *Philos. Trans. R. Soc. London, Ser. A*, **266**, 425–533, 1970.
- Lemon, E. R.(ed.), *CO₂ and Plants: The Response of Plants to Rising Levels of Atmospheric Carbon Dioxide*, AAAS Sel. Symp. Vol. 84, Westview Press, Boulder, Colorado, 1983.
- Levitus, S., *Climatological Atlas of the World Ocean*, NOAA Prof. Pap., **13**, Natl. Oceanic and Atmos. Admin., Washington, D.C., 1982.
- Lorenz, E. N., Climatic determinism, *Meteorol. Monograph.*, **30**, 1–3, 1968.
- Manabe, S., and K. Bryan, CO₂-induced change in a coupled ocean-atmosphere model and its paleoclimatic implications, *J. Geophys. Res.*, **90**, 11,689–11,707, 1985.
- Manabe, S., and R. J. Stouffer, Sensitivity of a global climate model to an increase of CO₂ concentration in the atmosphere, *J. Geophys. Res.*, **85**, 5529–5554, 1980.
- Manabe, S., and R. T. Wetherald, The effects of doubling the CO₂ concentration on the climate of a general circulation model, *J. Atmos. Sci.*, **32**, 3–5, 1975.
- Manabe, S., and R. T. Wetherald, Large-scale changes of soil wetness induced by an increase in atmospheric carbon dioxide, *J. Atmos. Sci.*, **44**, 1211–1235, 1987.
- McCormick, M. P., T. J. Swissler, W. H. Fuller, W. H. Hunt, and M. T. Osborn, Airborne and ground-based lidar measurements of the El Chichón stratospheric aerosol from 90°N to 56°S, *Geofis. Int.*, **23**, 187–221, 1984.
- Mearns, L. O., R. W. Katz and S. H. Schneider, Extreme high-temperature events: changes in their probabilities with changes in mean temperature, *J. Clim. Appl. Meteorol.*, **23**, 1601–1613, 1984.
- Mendonca, B. G. (Ed.), *Geophysical Monitoring for Climate Change*, No. 7, Summary Report 1978, 131 pp., NOAA Environ. Res. Lab., Boulder, Colorado, 1979.
- Miller, J. R., G. L. Russell and L. C. Tsang, Annual oceanic heat transports computed from an atmospheric model, *Dyn. Atmos. Oceans*, **7**, 95–109, 1983.
- Mitchell, J. M., A preliminary evaluation of atmospheric pollution as a cause of global temperature fluctuation of the past century, in *Global Effects of Environmental Pollution*, edited by S. F. Singer, pp. 139–155, Springer-Verlag, New York, 1970.
- Mossop, S. C., Volcanic dust collected at an altitude of 20 km, *Nature*, **203**, 824–827, 1964.
- National Academy of Sciences, *Understanding Climatic Change*, 239 pp., Washington, D.C., 1975.
- National Oceanographic and Atmospheric Administration, User's Guide to NODC Data Services, Environmental Data Service, Washington, D.C., 1974.
- Palmer, K. F., and D. Williams, Optical constants of sulfuric acid, Applications to the clouds of Venus?, *Appl. Opt.*, **14**, 208–219, 1975.
- Peixoto, J. P., and A. H. Oort, Physics of climate, *Rev. Mod. Phys.*, **56**, 365–429, 1984.
- Pollack, J. B., O. B. Toon, C. Sagan, A. Summers, B. Baldwin and W. Van Camp, Volcanic explosions and climatic change: A theoretical assessment, *J. Geophys. Res.*, **81**, 1071–1083, 1976.
- Ramanathan, V., R. J. Cicerone, H. B. Singh, and J. T. Kiehl, Trace gas trends and their potential role in climate change, *J. Geophys. Res.*, **90**, 5547–5566, 1985.
- Rind, D., R. Suozzo, N. K. Balachandran, A. Lacis, and G. Russell, The GISS global climate/middle atmosphere model, Part I Model structure and climatology, *J. Atmos. Sci.*, **45**, 329–370, 1988.

- Roberts, L., Coral bleaching threatens Atlantic reefs, *Science*, **238**, 1228-1229, 1987.
- Robinson, M., and R. Bauer, Oceanographic Monthly Summary **1**, No. 2, pp. 2-3, NOAA Natl. Weather Serv., W322, Washington, D.C., 1981.
- Robock, A., Internally and externally caused climate change, *J. Atmos. Sci.*, **35**, 1111-1122, 1978.
- Robock, A., A latitudinally dependent volcanic dust veil index, and its effect on climate simulations, *J. Volcanol. Geotherm. Res.*, **11**, 67-80, 1981.
- Russell, G. L., and J. A. Lerner, A new finite-differencing scheme for the tracer transport equation, *J. Appl. Meteorol.*, **20**, 1483-1498, 1981.
- Russell, G. L., J. R. Miller and L.C. Tsang, Seasonal oceanic heat transports computed from an atmospheric model, *Dynam. Atmos. Oceans*, **9**, 253-271, 1985.
- Schneider, S. H., and S. L. Thompson, Atmospheric CO₂ and climate: importance of the transient response, *J. Geophys. Res.*, **86**, 3135-3147, 1981.
- Schneider, S. H., and C. Mass, Volcanic dust, sunspots, and temperature trends, *Science*, **190**, 741-746, 1975.
- Shands, W. E., and J. S. Hoffman, (Ed.), *The Greenhouse Effect, Climate Change, and U.S. Forests*, 304 pp, Conservation Foundation, Washington, D.C., 1987.
- Smagorinsky, J., Carbon dioxide and climate: A second assessment. 239 pp, National Academy Press, Washington, D.C., 1982.
- Somerville, R. C. J., and L. A. Remer, Cloud optical thickness feedbacks in the CO₂ climate problem, *J. Geophys. Res.*, **89**, 9668-9672, 1984.
- Toon, O. B., and J. B. Pollack, A global average model of atmospheric aerosols for radiative transfer calculations, *J. Appl. Meteorol.*, **15**, 225-246, 1976.
- Walsh, J., and C. Johnson, An analysis of Arctic sea ice fluctuations, *J. Phys. Oceanogr.*, **9**, 580-591, 1979.
- Wang, W. C., G. Molnar, T. P. Mitchell, and P. H. Stone, Effects of dynamical heat fluxes on model climate sensitivity, *J. Geophys. Res.*, **89**, 4699-4711, 1984.
- Wang, W. C., Y. L. Yung, A. A. Lacis, T. Mo and J. E. Hansen, Greenhouse effects due to man-made perturbations of trace gases, *Science*, **194**, 685-690, 1976.
- Washington, W. M., and G. A. Meehl, Seasonal cycle experiment on the climate sensitivity due to a doubling of CO₂ with an atmospheric general circulation model coupled to a simple mixed-layer ocean model, *J. Geophys. Res.*, **89**, 9475-9503, 1984.
- Weiss, R. F., The temporal and spatial distribution of tropospheric nitrous oxide, *J. Geophys. Res.*, **86**, 7185-7195, 1981.
- Willson, R. C., and H. S. Hudson, Solar luminosity variations in solar cycle 21, *Nature*, **332**, 810-812, 1988.
- Willson, R. C., H. S. Hudson, C. Frohlich, and R.W. Brusa, Long-term downward trend in total solar irradiance, *Science*, **234**, 1114-1117, 1986.
- Wilson, C. A., and J. F. B. Mitchell, A 2xCO₂ climate sensitivity experiment with a global climate model including a simple ocean, final report CEC contract CL-114 UK (H), British Meteorol. Office, Bracknell, U.K., 1987.

I. Fung, J. Hansen, A. Lacis, S. Lebedeff, D. Rind, R. Ruedy and G. Russell, NASA Goddard Space Flight Center, Goddard Institute for Space Studies, 2880 Broadway, New York, NY 10025.

P. Stone, Center for Meteorology and Physical Oceanography, Massachusetts Institute of Technology, Cambridge, Massachusetts 02139.

(Received January 25, 1988;
revised May 6, 1988;
accepted May 6, 1988.)